Recent Advances in the Development of Materials for Terahertz Metamaterial Sensing

Suling Shen[a,b], Xudong Liu[a], Yaochun Shen[c], Junle Qu[b], Emma MacPherson[d], Xunbin Wei[e,f,g] and Yiwen Sun[a,]*

[a]National-Regional Key Technology Engineering Laboratory for Medical Ultrasound, Guangdong Key Laboratory for Biomedical Measurements and Ultrasound Imaging, Department of Biomedical Engineering, School of Medicine, Shenzhen University, Shenzhen 518060, China

[b]College of Physics and Optoelectronic Engineering, Shenzhen University, Shenzhen 518060, China

[c]Department of Electrical Engineering and Electronics, University of Liverpool, Liverpool L69 3GJ, UK

[d]Department of Physics, University of Warwick, Gibbet Hill Road, Coventry CV4 7AL, UK

[e]Biomedical Engineering Department, Peking University, Beijing, 100081, China

[f]Key Laboratory of Carcinogenesis and Translational Research (Ministry of Education/Beijing), Peking University Cancer Hospital & Institute, Beijing, 100142, China

[g]State Key Laboratory of Oncogenes and Related Genes, Shanghai Cancer Institute, Med-X Research Institute and School of Biomedical Engineering, Shanghai Jiao Tong University, 1954 Huashan Road, Shanghai 200030, China

[*]Corresponding author E-mail: ywsun@szu.edu.cn

Keywords: Terahertz sensing, Metamaterial, Surface plasmon polariton, Ultra-trace detection, Material selection

Abstract

Terahertz metamaterial sensing (TMS) is a new interdisciplinary technology. A TMS system employs terahertz waves as the pumping source and terahertz waves carry the substance information e.g. refractive index, absorption spectra in relevant to rotation and vibration states of molecular produced by a surface plasmon polariton like effect as the

Abbreviations. ATR: attenuated total reflection; BP: black phosphorus; CMOS: complementary metal–oxide–semiconductor; CNT: carbon nanotube; DAST: 4-N,N-dimethylamino-4′-N′-methyl-stilbazolium tosylate; FOM: figure of merit; ITO: indium tin oxide; MPA: metamaterial-based perfect absorber; PC: polycarbonate; PVDF: polyvinylidene fluoride; RIU: refractive index unit; SPP: surface plasmon polariton; SPR: surface plasmon resonance; SWCNT: single-walled carbon nanotube; TDS: time-domain spectroscopy; TMS: terahertz metamaterial sensing; TCH: tetracycline hydrochloride.

signal. TMS technology is usually characterized by large penetration depth and high sensitivity. Owing to these advantages, TMS may be used for ultra-trace detection and consequently has a wide range of practical applications in biomedicine, food safety, environmental monitoring, industry and agriculture, material characterization, and safety inspection. Furthermore, TMS performance is determined not only by the structural parameters of metamaterials, but also by their compositions and substrates. This paper reviews the essential fundamentals, relevant applications, and recent advances in TMS technology with a focus on the influence of material selection on TMS performance. We envisage this review to be used as a key reference for developing TMS-based functional devices with enhanced characteristics.

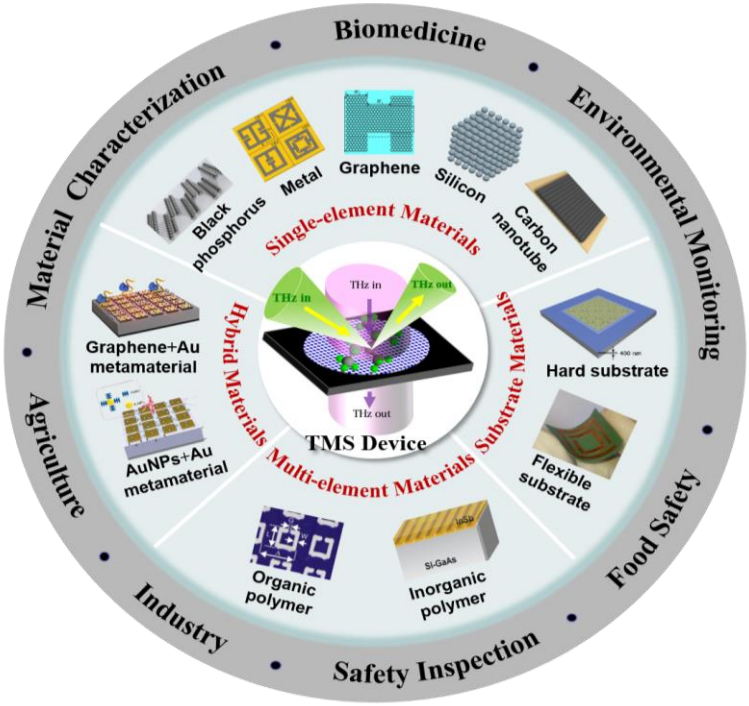

1. Introduction

Terahertz metamaterial sensing (TMS) combines the essential characteristics of terahertz

spectroscopy and metamaterials, in order to obtain better sensitivity (resonant frequency and the Q value of the resonant peak) for trace amounts to be detected. The research field of TMS has expanded rapidly, to the extent that it now touches many areas from fundamental science to real-world applications, for instance, biomedicine[1,2], food safety[3,4], environmental monitoring[5], industry and agriculture[6], material characterization[7], and safety inspection[8]. TMS is now recognized as an emerging technology. The fundamental concept of TMS technology is based on a surface plasmon polariton (SPP)-like effect, which explains the possibility of generating SPPs in the terahertz frequency range. This was originally discovered by Yen et al. in 2004[9]. The TMS process includes several elegant processes (see **Figure 1**). By considering the frequency-dependent interactions between the incident THz wave and the target substance on the metamaterial surface with the periodic subwavelength resonators, the substance properties (including the complex permittivity and conductivity) can be modulated because of the boundary condition modification in terahertz frequency. The resulting reflection and transmission signals encode the essential substance parameters, such as concentration[10], characteristic absorptions[11,12], refractive index[13], and rotational and vibrational modes of the functional groups[14], and can be extracted across the broadband terahertz spectrum. Moreover, the metamaterials specifically designed to resonate with the terahertz wave can be used to enhance the sample-wave interactions, thus increasing the TMS sensitivity[15,16]. Currently, many research groups are performing basic studies on TMS and its practical applications[17-26]. One of the most critical

characteristics that determine the performance of TMS is the sensitivity, which is highly dependent to the structure topology optimization of the metamaterials and selection of consisting materials. However, the majority of published works in this area have primarily focused on the structure topology optimization of the metamaterials rather than selection of consisting materials. A primary reason may be that the subject of metamaterials experienced a transitional stage, where the design theories and principles were gradually transformed into practical applications involving of selection of appropriate materials. Designing suitable metamaterials for highly sensitive TMS devices is more related to engineering applications, in which the properties of associated material play an important role.In this review, we highlight the recent advances in TMS technology in association with its main applications, with a focus on the effect of material selection on TMS performance.

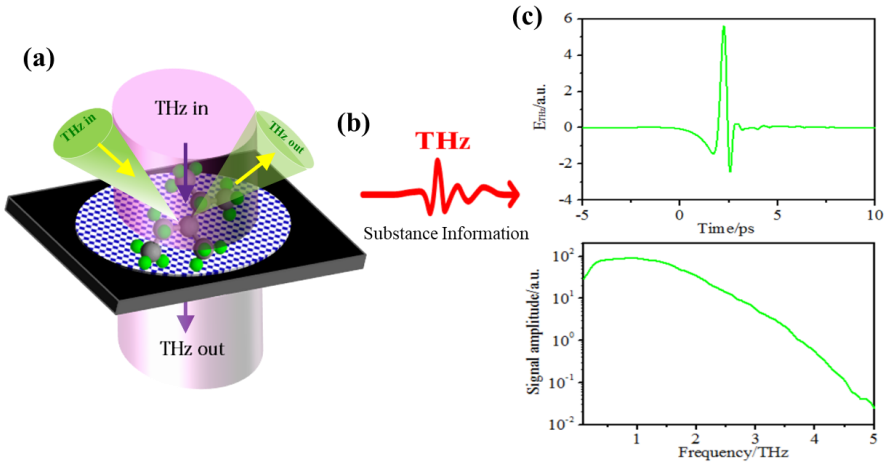

Figure 1: A physical model of the TMS process. (a) Interaction between the THz wave and the target substance on the metamaterial surface. (b) Generation and detection of the THz wave carrying substance information. (c) Parameter extraction under the frequency-dependent electromagnetic field.

2. Fundamentals

2.1 Terahertz Waves

The terahertz region of the electromagnetic spectrum lies between microwaves and far-infrared. It is typically defined as ranging from 0.1 to 10 terahertz in frequency or 3 mm to 30 μm in wavelength (**Figure 2**). This region has been historically referred to as a "terahertz gap" due to the lack of efficient generators and detectors. With the development of the advanced terahertz source and detectors working at ambient temperature, as well as commercial instrumentation like time-domain terahertz spectrometers (terahertz -TDS), terahertz science and technology has been extensively studied in the last few decades, and is becoming a thriving interdisciplinary area at the frontiers of science[12-14,27,28]. Terahertz waves have some unique characteristics that are very attractive. Unlike X-rays and microwaves, terahertz waves are non-ionizing and therefore safe for the target substance during low photon energy wave-material interactions[29,30], a property of utmost importance for bio-sensing. Moreover, terahertz waves are sensitive to the vibrational and rotational modes of many molecules[31] which are not detectable by conventional mid-infrared (MIR) spectroscopy. Furthermore, terahertz waves can penetrate non-polar substances and non-metallic materials (such as cloth, leather, and paper) easily[32], making non-destructive detection and analysis possible. In addition, terahertz instrumentation based on coherent detection methods measures the transient electric field, not simply its intensity, thus the absorption coefficient and refractive index of the sample are obtained from the amplitude and phase without requiring a Kramers-Kronig analysis. These properties have given rise to the field

of terahertz-Sensing[11,13,15,16,26]. However, challenges still exist, for example the weak response of terahertz waves to most natural materials and low spatial resolution/confinement of terahertz devices due to the diffraction limit. Therefore, there is increasing interest to enhance the interaction and the spatial resolution/confinement of terahertz waves with materials to achieve reliable sensing[33,34]. Using metamaterials is one of the most promising methods.

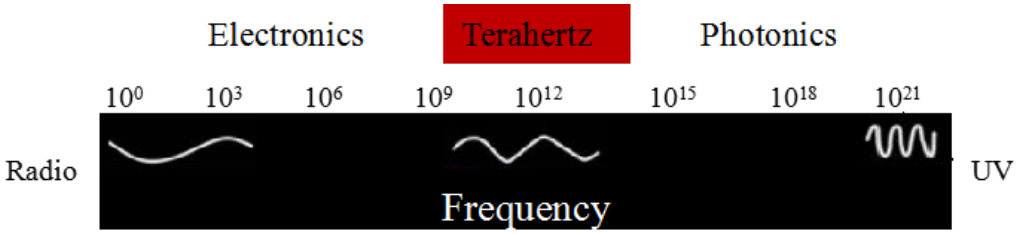

Figure 2: Location of the terahertz waves in the electromagnetic spectrum.

2.2 Metamaterials

The concept of metamaterials originated in 1968 from Veselago's theoretical prediction based on Maxwell's equations of the existence of materials with negative permittivity and permeability[35]. The extraordinary property of metamaterials is that the effective permittivity and permeability can be regulated by artificially designing a structure that is not possessed by natural materials. In 1996, Pendry et al. demonstrated negative effective permittivity in periodic metal wire arrays[36], and derived expressions for effective permittivity and the negative permeability, laying the theoretical foundation for the research of metamaterials[37]. Subsequently, the relationship between dielectric properties and structural design of metamaterials has been confirmed in numerous studies[38-41], which typically include left-handed materials[38], photonic crystals[39], and super-magnetic

materials[42] (**Figure 3**). Inspired by these iconic works, in 2009 Cui and Smith et al. experimentally realized a cloak under which an object can be hidden[41]. The extraordinary properties of metamaterials allow terahertz metamaterial sensing to go beyond the physical properties of natural materials with the high spatial confinement, and break the diffraction limit of terahertz waves. Therefore, terahertz metamaterial sensing has attracted attention because of its advantages of free-label detection and high sensitivity[1-8]. In addition, the remarkable characteristics of metamaterials in regulating amplitude, phase, polarization and impedance allow terahertz metamaterial sensing to exhibit potential applications in biomedical and other fields. However, the majority of earlier studies (mainly conducted by physicists) focused on the structure topology optimization of metamaterials rather than on material selection. In fact, proper selection of a functional material based on the principles of material science is required to obtain an ideal "metamaterial" system with expanded functionality and range of practical applications.

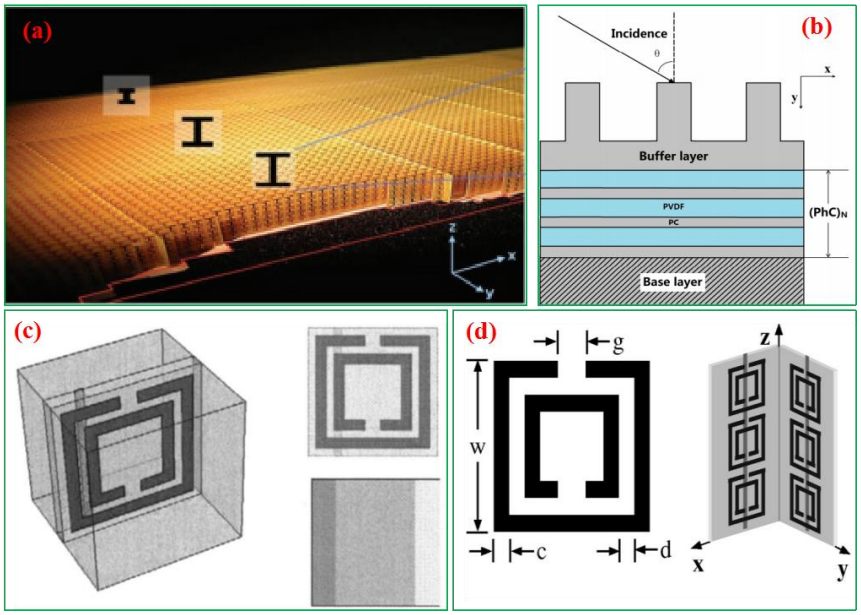

Figure 3: Various metamaterials including (a) a ground-plane cloak[41], (b) photonic crystals[39], (c) a split-ring resonator[42], and (d) a left-handed metamaterial[38].

2.3 TMS Technology

2.3.1 TMS Mechanism

Proper understanding of the underlying TMS mechanism is important for improving the TMS device performance. TMS sensitivity can be significantly increased by enhancing the electromagnetic resonance between the target and the sensing device, which consists of a low-frequency resonance and a high-frequency resonance. The low-frequency resonance is caused by the coupling between the material capacitance *C* and inductance *L*, whose frequency is expressed by equation (1)[43]. The high-frequency resonance of metamaterials refers to the plasmon resonance with the frequency expressed by equation (2)[44, 45].

$$\omega_{LC} = (\mathrm{LC})^{-0.5} = \frac{1}{\sqrt{L}\sqrt{\varepsilon_0 \int_0^{\nu} \varepsilon(\nu)\,\mathrm{E}(\nu)\,\mathrm{d}\nu}} \tag{1}$$

$$\omega_d \propto \frac{1}{2d\sqrt{\varepsilon_{eff}}} \quad (2)$$

$$\varepsilon_{\text{eff}} = \varepsilon_{sub} + \lambda\varepsilon_{air} + (1-\lambda)\varepsilon_a \quad (3)$$

where d is primarily determined by the geometric parameters of the metamaterial structure, ε_0 is the permittivity of vacuum, v is the space variable, $\varepsilon(v)$ is the material permittivity, E(v) is the electric field, and ε_{eff} is the effective dielectric constant of the testing environment depending on the target substance and metamaterial composition. The effective dielectric constant of the testing environment is expressed by equation (3), where ε_{sub}, ε_{air}, ε_a are the permittivity of the substrate, the permittivity of the air, and the permittivity of the analyte, respectively. λ is the volume ratio of air in the surrounding media. When the target substance and metamaterial composition change, the effective dielectric constant and related resonance frequency change as well. Therefore, both the structure topology and composition of a metamaterial have a direct impact on the resonant frequency of the corresponding TMS device.

The plasmon resonance modes induced by metamaterials in the terahertz range usually include toroidal-dipolar and Fano resonances[46,47]. Kaelberer et al. designed a multiple symmetrical metal split-ring resonator and successfully achieved a strong toroidal-dipolar resonance effect, as shown in **Figure 4(a)**[47]. In order to reduce the metal losses in plasmonic metamaterials, Li et al. confirmed this toroidal-dipolar resonance effect using a high-refractive-index dielectric metamaterial of LiTaO(3) micro-tube and obtained a high Q-factor in the terahertz regime (**Figure 4(b)**)[46]. In the mean time, Fano resonance mode widely exists in metamaterials which is first observed in asymmetric split ring arrays.

Both theory and experiment have confirmed that the Fano resonance effect in metamaterials can be realized by destructive interference among different excitation modes as shown in **Figures 4(c, d)**[48,49]**.**

According to the results of the literature studies cited above, the characteristics of the toroidal-dipolar, Fano, and capacitance-inductance resonances are closely related to the metamaterial structure. The majority of previous research on TMS focused on optimizing the device performance by designing suitable metamaterial structures[50-52]. However, the resonance frequency is determined not only by the metamaterial structure, but also by the effective dielectric constant of the surroundings, as indicated by equations (1) and (2). As a result, both the target substance and metamaterial composition need to be considered. Min and Huang have experimentally verified a hypothesis stating that the resonators made from different materials exhibit different resonance characteristics (**Figure 4(e)**)[53]. Therefore, proper material selection is required to obtain the ideal metamaterials with expanded functionality and application range based on the principles of material science by introducing various functional materials into the metamaterial structure.

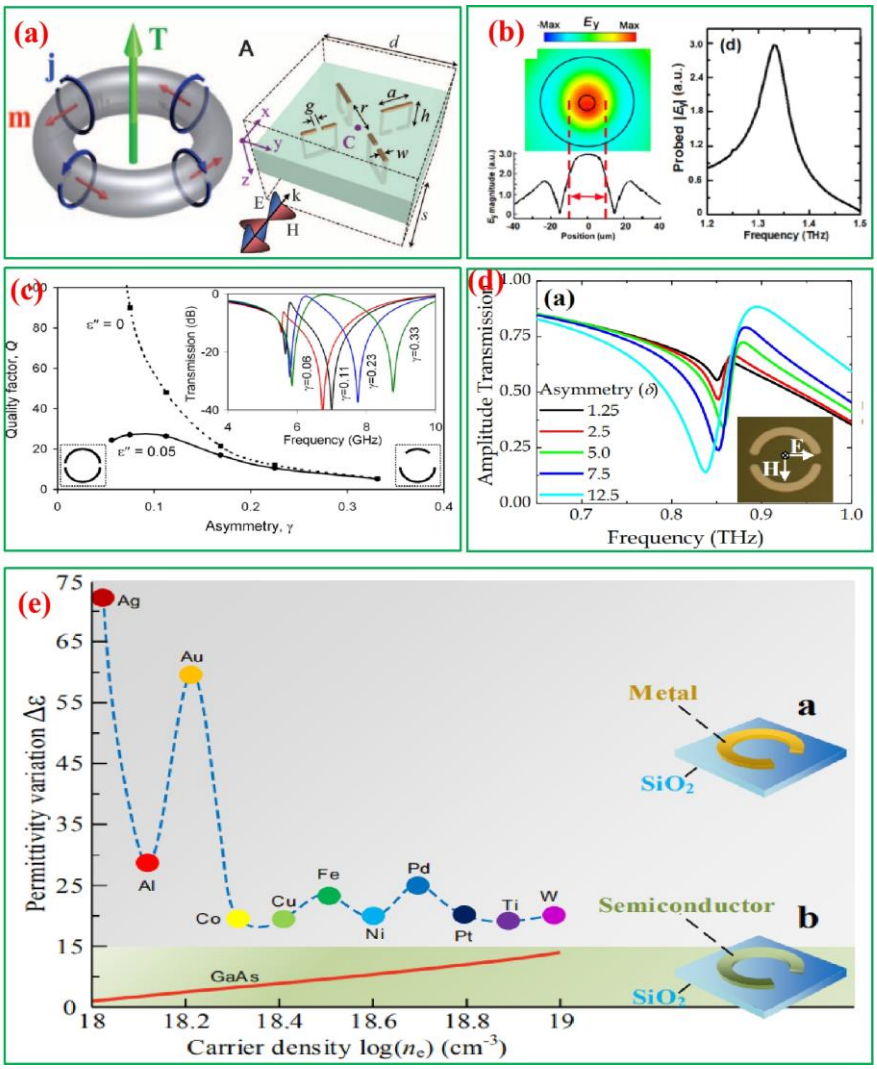

Figure 4: Toroidal-dipolar resonance induced by metamaterials in the works of (a) N. I. Zheludev[47] and (b) Z. Dong[46] Fano resonance induced by metamaterials in the works of (c) V. A. Fedotov[48] and (d) Ranjan Singh[49]. (e) Effective permittivity variations Δε obtained for the semiconductor (GaA; red solid line) and metallic (Ag, Al, Au, Co, Cu, Fe, Ni, Pd, Pt, Ti, and W; circles) metamaterials[53].

2.3.2 TMS Indexes

The main performance metrics of a TMS device include its sensitivity (S), quality factor (Q), and figure of merit (FOM). Sensitivity reflects the change in the resonance frequency with a change in the refractive index of the target substance[45]:

$$S = \frac{\Delta f}{\Delta n} \tag{4}$$

Note that $\triangle f$ is the change in the resonance frequency, and $\triangle n$ is the change in the refractive index; therefore, the unit of sensitivity is terahertz/RIU (refractive index unit). The quality factor Q reflects the resonance characteristics of the TMS device. Generally, Q can be expressed as[45]:

$$Q = \frac{f}{FWHM} \tag{5}$$

where f is the resonance frequency, and $FWHM$ is the full width at the half maximum of the resonance peak. Because TMS devices usually operate in different wavebands, the FOM value is typically used as a TMS device performance indicator[45]:

$$FOM = S \times Q \tag{6}$$

For more general applications, sensitivity can be linked with different physical parameters such as refractive index, concentration and thickness. Here we provide Table1 to summarize detection sensitivity till date. For example, Zhang et al indicated that the detection concentration sensitivity of sucrose solution is 0.03125 mol/L in the terahertz range based on a metasurface-enhanced aqueous solution sensor in Figure 5(a)[54]. J. Zhang et al proposed an ultrasensitive tunable terahertz sensor showing a frequency-sensitivity as high as 4.2 THz/RIU with FOM of 12.5 in Figure 5(b)[55]. Later, much research has proposed thickness sensitivity and wavelength-shift sensitivity as shown in **Figure 5(c-e)**[22,39,56].

Table 1: TMS indexes determined for different device configurations

TMS material	Frequency	Detection sensitivity	FOM (RIU^{-1})

Au [54]	1.7 Terahertz	0.47 Terahertz/RIU	49
Graphene [55]	2.3 Terahertz	12.66 μm/RIU	12.66
InSb [56]	0.43 Terahertz	146600 nm/RIU	NA
Au + Graphene [22]	0.95Terahertz	0.2 ng/L	N/A

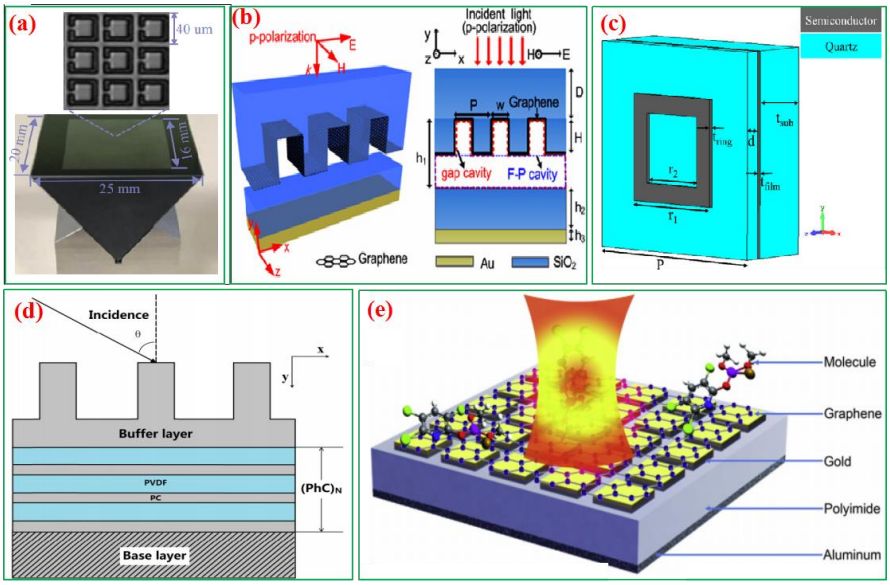

Figure 5: TMS configurations with different TMS indexes. (a) Complementary split rings with attenuated total reflection [54]. (b) Single-layer graphene-based gratings integrated with a Fabry-Perot cavity [55]. (c) A square-shaped perfect absorber [56]. (d) A dielectric multilayer consisting of nine alternating polycarbonate (PC, 7 μm) and polyvinylidene fluoride (PVDF, 5 μm) dielectric layers [39]. (e) A schematic of the monolayer graphene-coated Terahertz metamaterial [22].

3. From Elemental to Hybrid TMS Materials

3.1 Single-element Materials

3.1.1 Common and Noble Metals

Currently, the majority of metamaterials with desired properties are fabricated from common or noble metals (such as Au, Al, Ag, or Cu) that exhibit surface plasmon resonance (SPR) properties [1-3,19]. TMS based on these metals has been successfully used in biomedical science, environmental monitoring, and food safety applications. The

pressing issues of these areas require the development of a safe, accurate, and economical sensing technology[57]. The non-ionizing and nondestructive terahertz radiation technique can potentially meet these requirements. Multiple research studies have been devoted to optimizing the properties of TMS devices based on common or noble metals in the fields of environmental monitoring and food safety [3-6,54,58-60]. Singh et al. reported an aluminum metamaterial absorber operating at terahertz frequencies with enhanced sensitivity and high FOM value (**Figure 6(a)**) [5], which was effectively used in the fingerprint region of flammable and explosive molecules during environmental pollution studies. The majority of publications related to food safety applications is primarily focused on concentration estimations, chemical compositions, and the structures of antibiotics and allergens. Thus, Xie et al. applied Au metasurfaces to detecting trace amounts of antibiotic and chlorpyrifos-methyl molecules (**Figures 6(b, c)**) [3, 58]. However, many practical challenges related to the diffraction limit of terahertz waves and their strong absorption in polar solvents continue to impede TMS development. To eliminate these adverse effects, the analyzed sample volume must be decreased. For example, Serita et al. reported an Au terahertz microfluidic chip for detecting trace amounts of solution samples (**Figure 6(d)**) [60]. Using this device, they successfully analyzed trace amounts of glucose with a sensitivity of 1.4 fmol of solute in a 128 pL volume. MacPherson's group therefore designed and fabricated a highly sensitive multi-microfluidic-channel metamaterial sensor for terahertz sensing of small-volume liquid samples, **Figure 6(e)** [61]. Their design significantly decreases the amount of liquid

needed and enhances the interaction between the sensing targets and the terahertz light (thus increasing the sensitivity). This and other similar studies may accelerate the development of a TMS lab-on-a-chip technology.

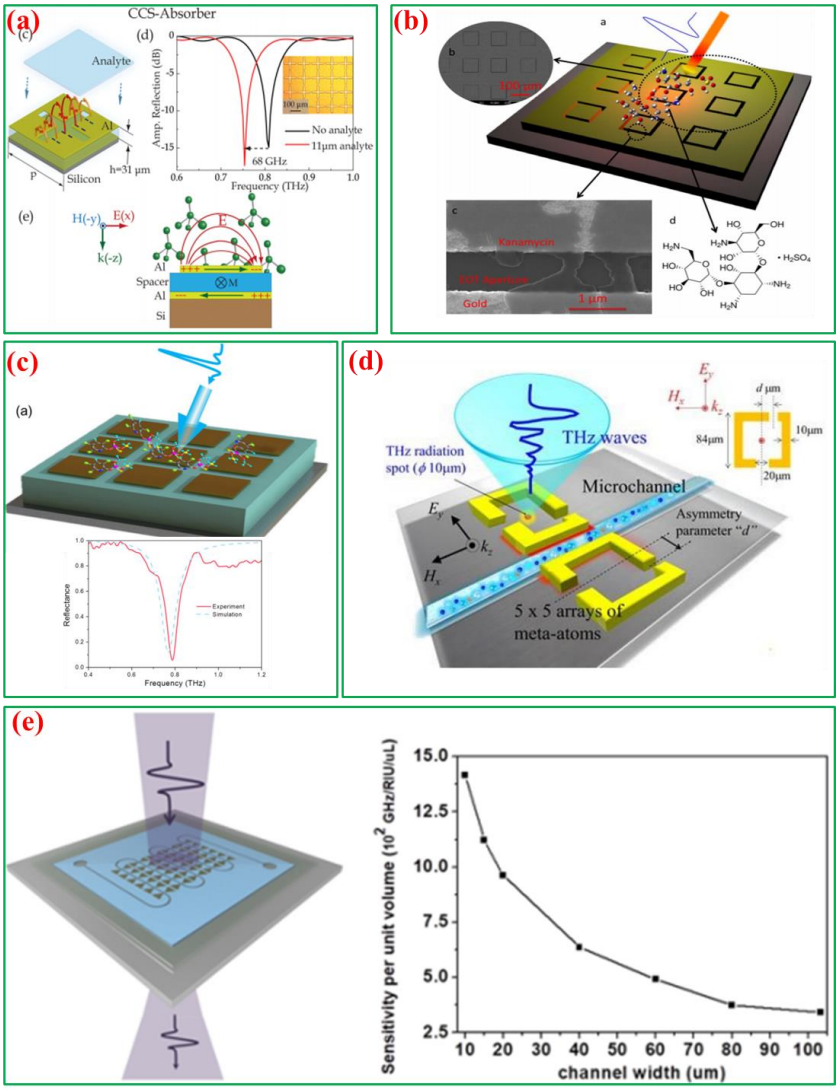

Figure 6: Terahertz common and noble metal-based metamaterials utilized in the environmental monitoring and food safety fields. (a) A complementary cross-shaped metamaterial absorber array [5]. (b) An array of square-shaped slits [58]. (c) Schematic diagram of terahertz metamaterials detection of chlorpyrifos-methyl [3]. (d) A terahertz microfluidic metamaterial [60]. (e) Microfluidic metamaterial biosensor for detection of small-volume liquid samples [61].

Terahertz technology has also attracted significant interest in the area of biomedical sensing as the collective vibration modes of many biomolecules can be predicted with high accuracy in the terahertz regime. The terahertz metamaterials based on common or noble metals are employed for high-sensitivity sensing and accurate discrimination in biomedical applications [62] related to the detection of proteins [62-65], cancer cells [2,26,66], DNA molecules[67], viruses[68], and microorganisms[69] as well as in medical diagnosis[1,70,71]. For example, Yang et al. prepared a planar array of highly sensitive Au split-ring resonators for the discrimination of the wild-type and transgenic genome DNA molecules (**Figure 7(a)**) [67], while Park et al. demonstrated highly sensitive detection of viruses using the Au split-ring resonators depicted in **Figure 7(b)** [68]. However, the main challenge related to the TMS application in biomedical science is the strong absorption of terahertz waves in polar solvents (such as water), which makes it difficult to accurately extract information for solute molecules [72]. To address this issue, TMS was integrated with microfluidic technology, which allowed a small amount of liquid to pass through[2,64]. Specifically, Geng et al. developed an Au terahertz metamaterial biosensor integrated with a microfluidic channel to detect a biomarker of liver cancer in its early stage with a detection concentration of 25.24 pg/L (**Figure 7(c)**) [73]. Another well-known technique that is capable of overcoming the negative effects produced by the polar solvent absorption in the terahertz regime is attenuated total reflection (ATR) [74]. K. Tanaka and co-workers developed Au terahertz metamaterials using split-ring resonators with increased resonance, as shown in the corresponding ATR spectrum (**Figure 7(d)**) [74,75].

Recently, A. Ahmadivand's group designed an approach to detect SARS-CoV-2 virus protein at low level using toroidal THz metamolecule which makes COVID-19 infection diagnosis easy[76]. However, TMS based on common and noble metals exhibits limited frequency tunability when applied to studying fixed structures, which in turn causes various problems during the multi-frequency investigations required for material characterization and bio-related applications. Table 2 summarizes the recent applications of TMS based on noble metals. For example, TMS based on common and noble metals has a wide range of practical applications in THz sensing, biomedicine, food safety and environmental monitoring with relatively high sensitivity. Besides TMS, many sensors such as optical plasma sensors have applications in the above field with high sensitivity[77-79]. However, TMS system employs terahertz waves as the pumping source; but optical plasma sensors employs optical waves as the pumping source. The complementary penetration depth makes them suitable for different application scenarioes.

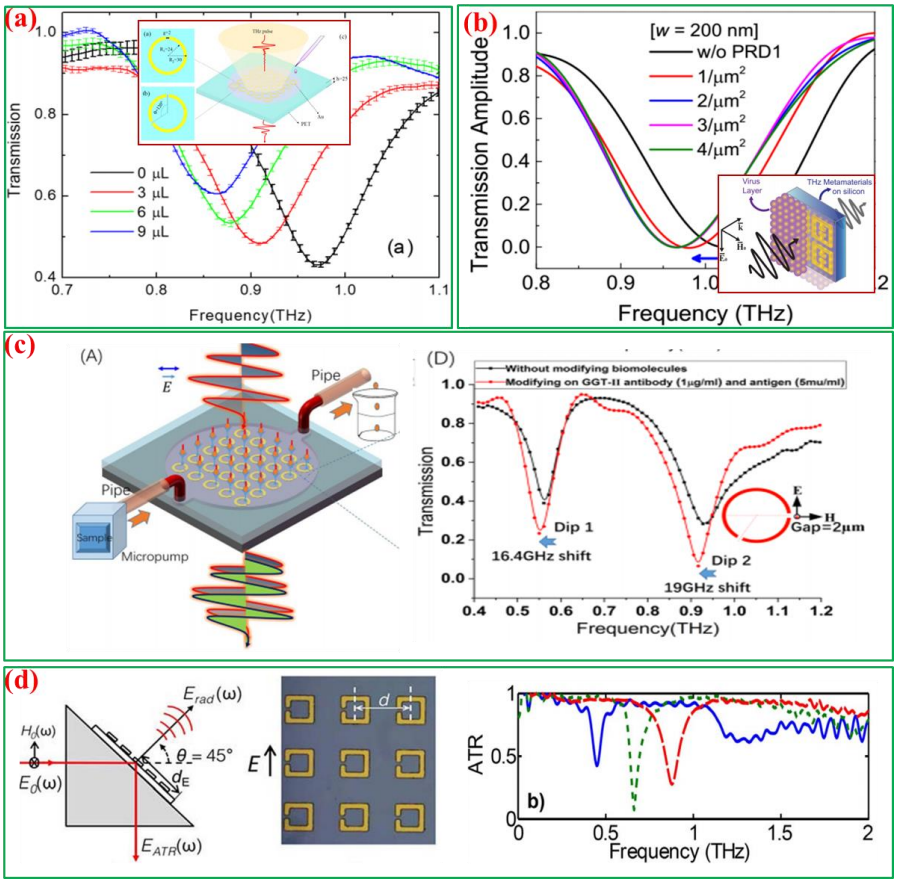

Figure 7: Terahertz common and noble metal-based metamaterials utilized in biomedical science. (a) A planar array of Au split-ring resonators [67]. (b) Terahertz split-ring resonators with nano-gap widths [68]. (c) A Terahertz metamaterial Au chip biosensor integrated with a microfluidic channel [73]. (d) Split-ring resonators combined with the ATR technique [74].

Table 2: Recent TMS applications utilizing common and noble metals (Au, Al, Ag, Cu)

	Target	Technique	Main results	Materials and reference
Terahertz sensing	N/A	Fano resonance	S = 0.08 Terahertz/RIU	Au [80a]
	Invisibility cloaks	Gradient metasurface	Ultra-thin carpet cloak	Cu + Au [81a,b]
	N/A	Ultra-thin resonator	High absorptivity	Cu [82a]
	N/A	Parallel plate waveguide	Apparent frequency shift	Metal [83a]
	Photoresist	Quadrupole and Fano resonances	S =5.7×10^4 nm/RIU	Al [84a]
	Thin films	Dual-band absorber	S = 0.187 Terahertz/RIU	Ag [15a]
	Thin films	Split-ring resonator	Ultra-thin sensing	Al [16a]
	Thin films	Hole array	FOM = 153.7 mm^{-1}	Al [85a]

	N/A	Flexible absorber	Absorption of 99%	Au [58b]
Food safety	Chlorpyrifos methyl	High transmission	*S* = 1 g/L	Au [3b]
	Allergens	Metasurfaces	High sensitivity	Au [54a,b]
	Sucrose solutions	ATR	*S* = 0.03125 mol/L	Cu [59a,b]
	Lactose and fructose	Split-ring resonator	*S* = 20 mg/mL	Au [60a,b]
	Sugar solutions	Microfluidic channel	*S* = 1.4 fmol in 128 pL	Au [4a,b]
	TCH	circular rings array	*S*= 0.1 mg/L	Al [5a]
Environment	Explosive molecules	Metamaterial absorbers	Improved sensitivity	Al [63a], Cu [64a,b]
Biomedical science	BSA solutions	Square-ring resonator	*S* = 5 mg/mL	Au [71a,b]
	Organ tissues	Metamaterial resonator	Wide-band frequency selection	Au [67a,b]
	Transgenic genome	Au split-ring array	Label-free discrimination	Au [68a,b]
	Virus layers	Split-ring resonator	*S* = 80 GHz·μm^2/particle	Au [65a,b]
	Cancer biomarkers	Microfluidic channel	14.2 GHz resonance shift	Au [66a,b]
	Oral cancer cell apoptosis	10-μm-thick polyimide substrate	Linear relationship between cell apoptosis and change in resonant frequency	Au [26a,b]
	Oral cancer cells	Double split-ring resonator	*S* = 900 kHz/cell mL^{-1}	Al [86a,b]
	Glucose and ethanol	Microfluidic channel	S = 3.5 Terahertz/RIU	Metal [70a]
	Medical diagnostics	Cavity / resonator modes	Full control of the sensor response	Metal [69b]
	Microorganisms	Frequency selective surface	Sensitivity up to 20%	Au [80a]
	SARS-CoV-2 spike proteins	Toroidal THz metamolecule	Sensitivity up to 4.2 fM	Au [76a,b]

[a] (simulation); [b] (experiment)

3.1.2 Two-dimensional Single-element Materials (Graphene, Carbon Nanotubes, and Black Phosphorus)

The TMS methods based on the SPPs generated on the surfaces of common and noble metals (Au, Ag, Cu, and Al) have been extensively studied by researchers [64-86]; however, they suffer from large intrinsic losses and non-tunability. Recently, two-dimensional single-element materials (such as graphene, carbon nanotubes (CNTs), and black

phosphorus (BP)) have attracted considerable attention as potential TMS materials due to their unique electrical and optical properties. Furthermore, these materials support well-confined SPPs in the terahertz frequency range at high doping levels [87-92]. In particular, the TMS techniques utilizing two-dimensional single-element materials exhibit high sensitivity and detection accuracy; they also demonstrate good dynamic tunability by electrostatic gating and smaller intrinsic losses in resonance, which may represent a more flexible alternative to the TMS methods based on conventional common and noble metals.

Graphene

TMS with high dynamic tunability is essential for real world applications. TMS based on graphene can be tuned by varying the conductivity of the graphene through an electrical gate. Our group has designed and verified the tunability of graphene based terahertz light modulator in total internal reflection geometry, which reached a maximum of 99.3% at 0.24 THz shown in **Figure 8(a)** [93]. This technique thus could be developed into a very powerful tool for sensing. Terahertz graphene-based metamaterials can be potentially applied to the sensing of hazardous gases due to their unique two-dimensional characteristics and very large surface areas[94]. For example, Jha and co-workers proposed ATR-based gas sensors operating in the terahertz frequency range that contained free-standing doped graphene monolayers (**Figures 8(b, c)**) [95,96]. These gas sensors possessed an ultrahigh sensitivity of 34.11°/RIU and FOM of more than 1150 RIU^{-1} with the capability of dynamically tuning their SPP spectra by chemical or electrical doping.

Xiang et al. also presented a highly sensitive gas sensor operated at terahertz frequencies by exciting the SPR of graphene with a sensitivity of 147°/RIU (**Figure 8(d)**) [97]. The results of these studies indicate that graphene-based TMS techniques are characterized by the high sensitivity and dynamic tunability for detecting and identifying hazardous gases.

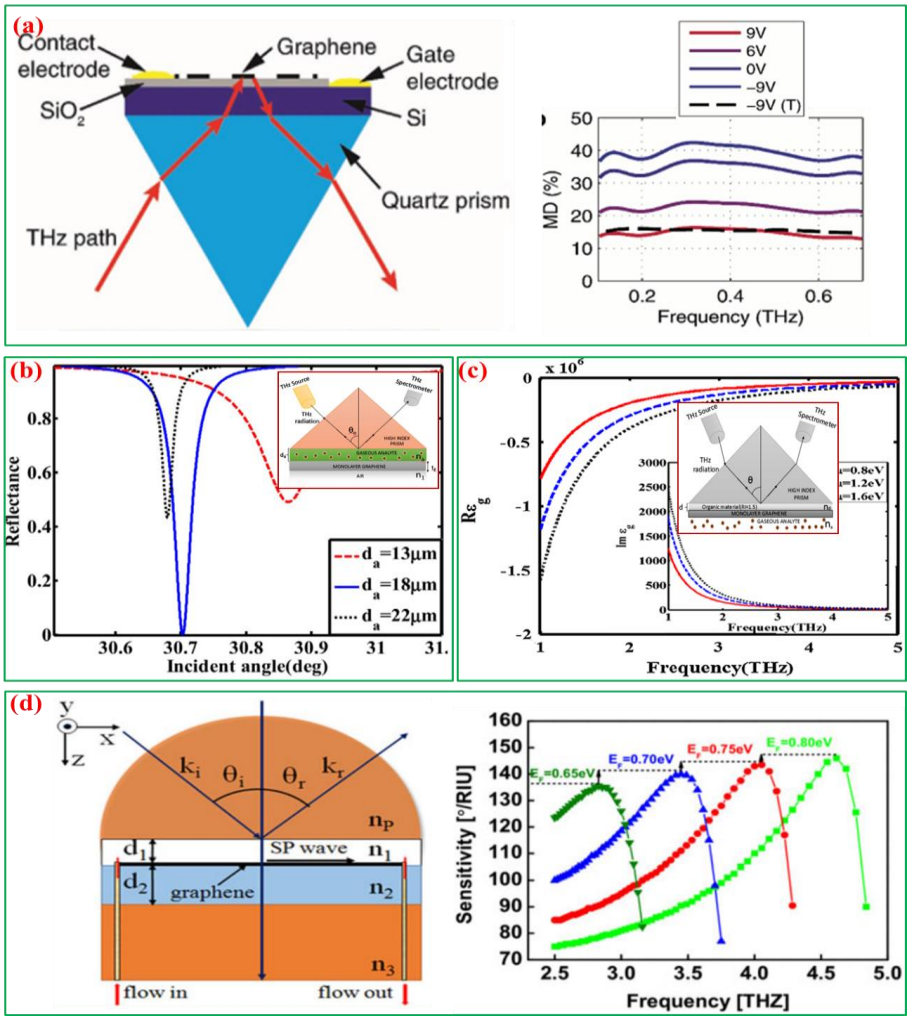

Figure 8: (a) Graphene based terahertz light modulator in total internal reflection geometry [93]. Terahertz graphene-based metamaterials used in hazardous gas sensing applications:(b) An Otto configuration combined with the ATR technique that contains a free-standing doped graphene monolayer [95]. (c) An SPR-based gas sensor with a doped graphene monolayer combined with the ATR technique via a modified Otto coupling configuration [96]. (d) An SPR-based graphene-containing gas sensor [97].

Terahertz graphene metamaterials can also be potentially utilized for biomedical sensing

because of their large specific areas and good adsorption properties[96]. Tang et al. theoretically investigated graphene-based split-ring resonators with tunable frequencies and amplitudes (**Figure 9(a))** [98]. Xiang et al. proposed a similar dynamically tunable resonator containing an H-shaped graphene layer with an FOM value of 17.78 (**Figure 9(b)**) [99]. Furthermore, Song et al. examined a three-dimensional graphene metamaterial structure that was highly sensitive to changes in the analyte refractive index and thickness (**Figure 9(c**)) [100]. These configurations may help to design ultra-sensitive terahertz metamaterial sensors for the real-time on-chip chemical and biomolecular detection. In addition, the terahertz biomedical sensors based on the graphene metamaterials with excellent absorption properties were developed as well. For example, Wu et al. reported a graphene nanoribbon ring cross structure with a theoretical absorption of 99.8% and FOM of 12.66 (**Figure 9(d)**) [101]. Similarly, Fan et al. constructed a terahertz dual-band absorber with a periodic cross-shaped graphene pattern (**Figure 9(e)**)[102]. These absorbers exhibit very high adjustability and can be applied in terahertz metamaterial biomedical sensing. The core design criterion for such sensors was the maximization of interactions between the incident light and the analyte to achieve ultra-high sensitivity and high sensing resolution. However, because the interactions between terahertz radiation and the majority of analytes were very weak, it was difficult for many terahertz sensors to reach the sensitivity and resolution levels typical for optical sensing applications. To further enhance the sensitivity and resolution properties of terahertz sensing, Yan et al. proposed an ultra-sensitive high-resolution tunable terahertz sensor

consisting of single-layer graphene-based gratings integrated with a Fabry-Perot cavity (**Figure 9(f)**) [55]. Using this sensor, a frequency sensitivity of up to 4.2 terahertz per refractive index unit and FOM beyond 12.5 in the terahertz regime were achieved. Owing to the high tunability and smaller intrinsic losses of graphene as compared with the corresponding parameters of metal plasmonics, the former material represents the most promising alternative for the development of on-chip integrated terahertz biochemical sensors. Table 3 summarizes the recent applications of the graphene-based TMS technology. It can be concluded from table 3 that TMS based on graphene has high sensitivity and detection accuracy. In addition, due to the electrically-adjustable conductivity of graphene, TMS based on graphene with high dynamic tunability is essential for more practical applications. However, graphene also has a disadvantage due to its non-robust characteristics, which will inevitably lead to higher cost of TMS and therefore limit the potential application. Therefore, researchers must find ways to make the performance of graphene more stable and robust.

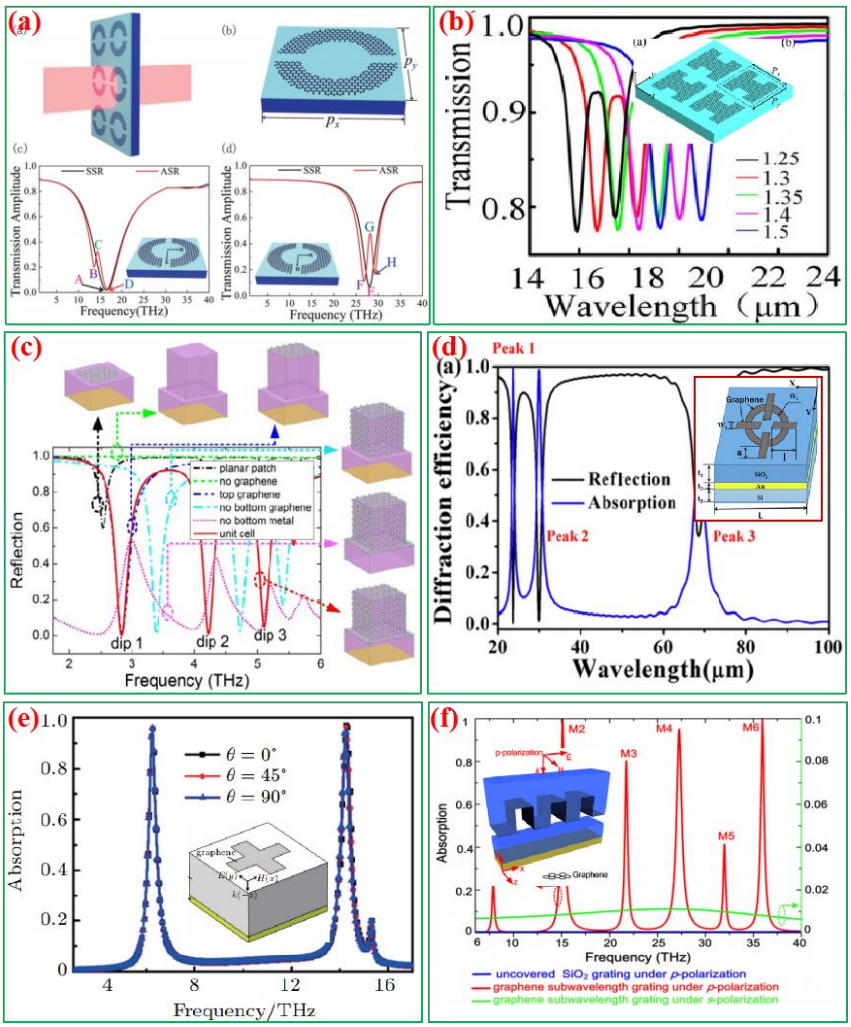

Figure 9: Graphene-based Terahertz metamaterials utilized in biomedical science. (a) Dynamic metamaterial based on a graphene split-ring high-Q Fano resonator [98]. (b) Dynamically tunable resonator containing an H-shaped graphene layer [99]. (c) A three-dimensional graphene metamaterial structure [100]. (d) A perfect metamaterial graphene multi-band absorber containing a nanoribbon ring cross [101]. (e) A dual-band graphene metamaterial absorber with a periodic cross-shaped pattern [102]. (f) An ultra-sensitive tunable Terahertz sensor with a graphene plasmonic grating [55].

Table 3: Recent applications of the graphene-based TMS techniques

	Graphene			
	Target	Technique	Main results	Reference
Terahertz	N/A	Fano resonance	Dynamically tuned shape and location	[103[a]]
	N/A	Localized plasmon resonances	Wide-angle beam with a high reflection efficiency of 60%	[104[a]]
	N/A	Multi-band absorbers	Absorption of 99.9% at	[105[a]]

			1.08 Terahertz	
	N/A	Perfect absorber	Absorption of 99.9% at 1.865 Terahertz	[106[a]]
Environmen	Gaseous analytes	ATR	S = 34.11°/RIU	[95[a,b]]
	Gaseous analytes	ATR	High sensitivity and detection accuracy	[96[a]]
	Gaseous analytes	SPR	S = 147°/RIU	[97[a]]
Biomedical science	Water	Fano resonance	S = 3260 RIU^{-1}	[87[a,b]]
	Protein monolayers	Plasmon resonance	High-sensitivity tunable plasmonic biosensor	[107[a,b]]
	Thin films	Graphene plasmonic grating	Frequency sensitivity of 4.2 Terahertz/RIU	[55[a]]
	Thin films	Multi-band absorber	FOM = 12.66	[100[a,b]]
	Biomolecules	Wire-slot and split-ring resonators	S = 177.7 GHz/RIU and FOM = 59.3	[108[a]]
	Thin films	Fano and quadrupole resonances	S = 2.12139 Terahertz RIU^{-1}	[98[a,b]]
	Thin films	H-shaped graphene resonator	S = 8 μm/RIU FOM = 17.78	[99[a]]
	Biomolecules	Multiple plasmonic resonances	S = 1.643 Terahertz/RIU	[109[a,b]]
	N/A	Terahertz dual-band absorber	FOM = 15.3	[102[a]]
	DNA	THz metasurface with microfluidic cell	S = 100 nM DNA	[110[a,b]]

[a] (simulation); [b] (experiment)

CNTs

The single-walled CNTs rolled from a graphene sheet possess excellent chemical and environmental stabilities and good tunability characteristics [111]. More specifically, the large mean free path and extraordinary electronic properties of CNTs make them particularly suitable for detecting terahertz modulations [112]. Nikolaenko et al. reported the exceptional nonlinear optical properties of a CNT metamaterial in the terahertz spectral range (**Figure 10(a)**) [90]. Xu et al. developed a mechanically tunable terahertz sensor containing stretchable buckled carbon nanotube sheets on a natural rubber

substrate (**Figure 10(b)**) [89]. Park et al. investigated the transmission of terahertz waves through an array of nanogaps with variable dimensions and periodicities to demonstrate the terahertz sensing of a thin film of single-walled CNTs (**Figure 10(c)**)[113]. Not satisfied with detecting only external modulations, Wang et al. performed a terahertz sensing of methyl chlorpyrifos using CNT metamaterials (**Figure 10(d)**)[114]. The achieved detection sensitivity was better than 0.1 mg/L, which was lower than the World Health Organization's provisional guideline limit established for the content of methyl chlorpyrifos in vegetables. Table 4 summarizes the recent applications of CNT-based TMS techniques and the results of the cited terahertz spectroscopy studies can help in the development of highly sensitive TMS devices due to the relative ease of fabricating CNT metamaterials and their robust flexible properties.

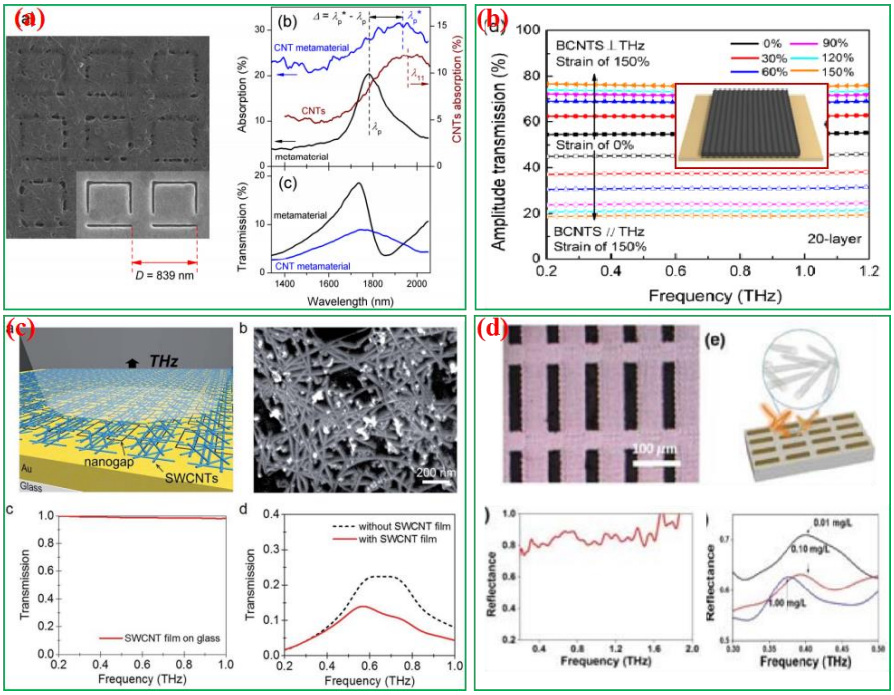

Figure 10: CNT-based Terahertz metamaterials for sensing applications. (a) Single-walled CNT (SWCNT) metamaterial [90]. (b) Stretchable buckled CNT sheets [89].

(c) A SWCNT film containing 2 nm wide gaps along a rectangular loop [113]. (d) A schematic diagram of the CNT TMS application [114].

Table 4: Recent applications of the CNT-based TMS techniques

CNT				
Applications	Target	Technique	Main results	Reference
Terahertz sensing	Strains	Stretchable buckled CNTs	Highly sensitive strain sensing	[89[a,b]]
	NA	CNT metamaterials	Modulation depth of 10%	[90[b]]
Biomedical science	Thin films	3D fishnet metamaterial	Tunable sheet resistance	[115[a,b]]
	Methyl chlorpyrifos	CNT metamaterials	*S*= 0.1 mg/L	[114[b]]
	Biomedical molecules	Strong Terahertz resonances	Amplitude transmission of 50%	[113[a,b]]

[a] (simulation); [b] (experiment)

BP

In recent years, BP has been an emerging member of the family of two-dimensional materials, owing to its large tunable electronic bandgap and high electron mobility[91,92,116-122]. The utilization of BP in TMS applications is still in its early stage, and the majority of published works on this topic mainly involve theoretical simulations[117]. Liu and Aydin theoretically investigated the localized SPRs generated in a nanostructured BP monolayer (**Figure 11(a)**) [121], which demonstrated that BP could also be used to build metamaterial sensors operating at terahertz wavelengths. Fo et al. enhanced the signal response of a nanostructured BP monolayer in the terahertz frequency range and examined the localized SPRs generated in BP nanostrip arrays (**Figure 11(b)**) [91]. The plasmonic resonances studied in that work strongly depended on the geometric parameters of nanostrips and coupling between the adjacent nanostrips, indicating that BP monolayers were outstanding candidates for TMS applications. At the

same time, Qing et al. designed a metamaterial perfect absorber composed of a BP monolayer (**Figure 11(c)**)[92]. Wang et al. proposed a dual-controlled switchable broadband metamaterial absorber consisting of BP and vanadium dioxide and operating at terahertz frequencies (**Figure 11(d)**)[122]. The enhanced absorption of the tunable BP-based absorber and its easy-to-fabricate structure are advantageous in terms of potential TMS applications. Although the research on BP metamaterial sensing is still in its early stage, and the trade-off between the performance and device cost remains a considerable challenge[117], BP is likely to become an outstanding material for the ultra-sensitive metamaterial sensors operating at terahertz frequencies. Table 5 summarizes the recent applications of BP-based TMS techniques. For instance, the exploitation of BP for detection of THz waves is now still at its early stage considering of all works about BP-based TMS techniques are simulation. Anyway, the certain optoelectronic properties of BP makes it well suited for novel THz applications and good to realize tunable BP-based TMS devices.

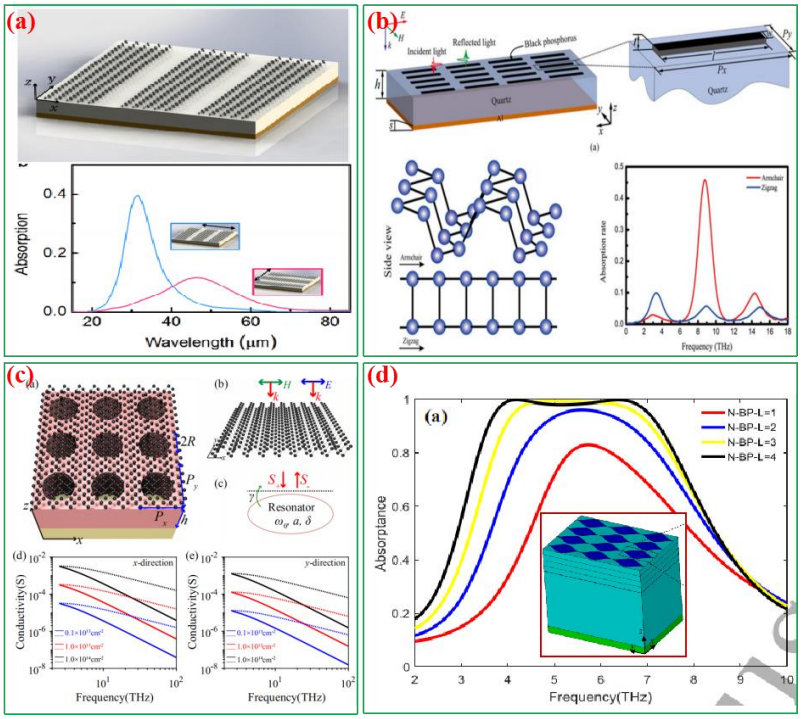

Figure 11: Terahertz BP-based metamaterials for sensing applications. (a) Localized SPRs generated in a nanostructured BP monolayer [121]. (b) Schematic of the periodic BP nanostrip array and dimensions of the BP nanostrip unit cell [91]. (c) A metamaterial perfect absorber composed of the BP monolayer with frequency-dependent surface conductivity[92]. (d) Schematic of the BP-based sandwich-structured absorber and its electronic properties [122].

Table 5: Recent applications of the BP-based TMS techniques

BP				
Applications	Target	Technique	Main results	Reference
Terahertz sensing	N/A	BP absorber	Absorption > 90%	[116[a]]
	N/A	BP localized surface plasmon resonances	Absorption approached 0.51 in the armchair direction	[91[a]]
	N/A	Perfect absorber	Q = 95.1	[92[a]]
	N/A	BP localized surface plasmon resonances	Anisotropic absorption properties	[121[a]]
	N/A	Broadband tunable BP absorber	Tunable absorbance from 34.64 to 98.8%	[122[a]]

[a] (simulation); [b] (experiment)

3.1.3 Silicon

The terahertz sensing techniques using metallic metamaterial-based perfect absorbers

(MPAs) have been extensively studied over the past few years[123]. However, metallic MPAs suffer from several drawbacks, such as relatively narrow bandwidths and high ohmic losses in the material[124]. Recently, silicon-based plasmonic MPAs have attracted much attention because of their ability to be easily incorporated into silicon-based platforms using the existing complementary metal-oxide-semiconductor (CMOS) technology with tunable broadband characteristics[124-132]. Fan et al. fabricated a silicon-based terahertz metamaterial absorber containing a cylinder array (**Figure 12(a)**)[129]. Zhao et al. and Liu et al. proposed an ultra-wideband silicon-based terahertz metamaterial absorber with an optically tunable peak absorbance over 99% (**Figures 12(b, c)**)[124,125], which could be operated across a wide range of the incident angles at terahertz frequencies. Wang et al. reported two silicon-based plasmonic metamaterial absorbers with absorption rates of 99.7% and 99.9%, which could be used as terahertz metamaterial sensors for detecting chlorpyrifos (**Figure 12(d)**) [127]. Clear shifts in the absorption spectra were observed after the deposition of chlorpyrifos (whose detectable concentrations were as low as 0.1 ppm) using the silicon-based plasmonic metamaterial absorber. Table 6 summarizes the recent applications of silicon-based TMS techniques, from which we can see more work is required to increase the sensitivity and application range of this device. However, the silicon-based absorber acted as a high-sensitivity sensor, demonstrating a considerable potential of detecting trace pesticides.

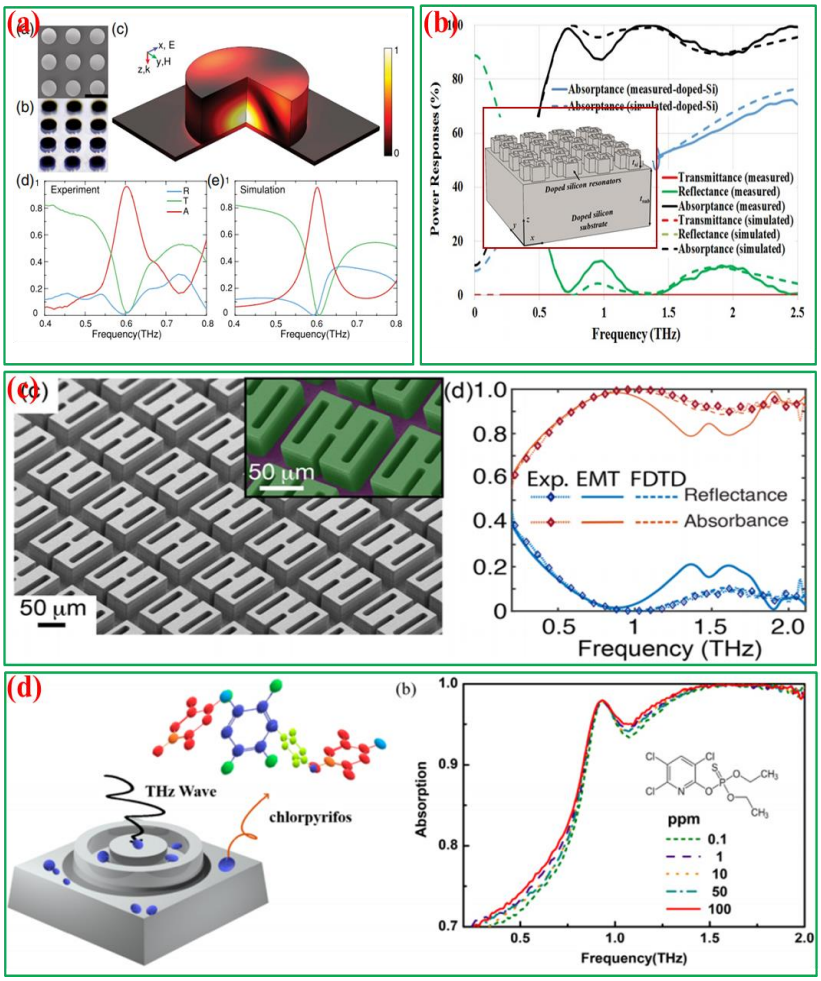

Figure 12: Terahertz silicon-based metamaterials used in sensing applications. (a) A cylinder array absorber fabricated by W. J. Padilla [129]. (b) An all-dielectric Terahertz absorber containing doped silicon, which was developed by F. Hu [125]. (c) A single-layer H-shaped all-silicon array Terahertz perfect absorber fabricated by X. Zhang [124]. (d) A Si-based plasmonic metamaterial absorber proposed by Y. Wang [127].

Table 6: Recent applications of silicon-based TMS techniques

Application	Target	Technique	Main results	Reference
Terahertz sensing	N/A	Terahertz perfect absorber	Absorbance exceeds 99%	[124[a,b]]
	N/A	All-dielectric Terahertz absorber	Absorbance of 95%	[125[a,b]]
	N/A	All-dielectric metasurface absorber	Absorbance of 96%	[129[a,b]]
Food safety sensing	Trace pesticides	All-dielectric resonator	Absorbance of 99.9% S = 0.1 ppm	[127[a,b]]

[a] (simulation); [b] (experiment)

3.2 Multi-element Materials

3.2.1 Inorganic Compound Materials

Inorganic compound semiconductors are advantageous over other semiconductor types because their plasma frequencies can be actively tuned by varying the carrier concentration; they also exhibit low adsorption losses and manufacturing costs [56,133]. Consequently, multiple studies have been performed to explore possible TMS applications of inorganic compound materials including InAs [134], InSb [135,136], indium tin oxide (ITO)[137], and perovskites[138,139]. Specifically, Bai et al. demonstrated theoretically that a tunable slow light effect could be realized in the planar InSb metamaterials composed of split-ring resonators and cut wires in a broad terahertz range (**Figure 13(a)**)[133]. Wang et al. proposed a multi-band terahertz sensing device consisting of a split-ring resonator with a perovskite hybrid structure (**Figure 13(b)**) [139]. However, the experimental implementation of the fast and precise polarization sensors is difficult, which considerably limits their practical applications. Therefore, Peng et al. described an innovative indium phosphide (InP) terahertz metamaterial sensor that used nanotechnology for conducting full-scale terahertz polarization measurements (**Figure 13(c)**)[140], which could be easily realized in scientific and industrial applications. In addition, Chochol et al. examined a terahertz SPR sensor based on InSb and InAs compounds with tunable sensitivities to different dielectric materials (**Figure 13(d)**) [134]. Aslinezhad proposed theoretically as well as numerically a highly sensitive refractive index and temperature sensor containing InSb metamaterial and operating in the terahertz

frequency range (**Figure 13(e)**) [56]. The obtained perfect absorber exhibited a refractive index sensitivity of 146600 nm/RIU and temperature sensitivity of 7144 nm/K. Our group innovatively showed that ITO-based CSRR metasurfaces can excite multi-peaks resonance in 0.1–2 THz by numerical simulation and experimental measurements (**Figure 13(f)**) [141]. The optically transparent ITO-based THz metasurface may become suitable for such purposes by providing a transparent platform for the simultaneous implementations of photodynamic therapy and THz bio-sensing. Table 7 summarizes the recent applications of the TMS techniques based on inorganic compound materials. The inorganic compound metamaterial structures described in this section have considerable TMS application prospects due to their good tunability and relatively low adsorption losses, although more studies are required to expand the application range of these devices.

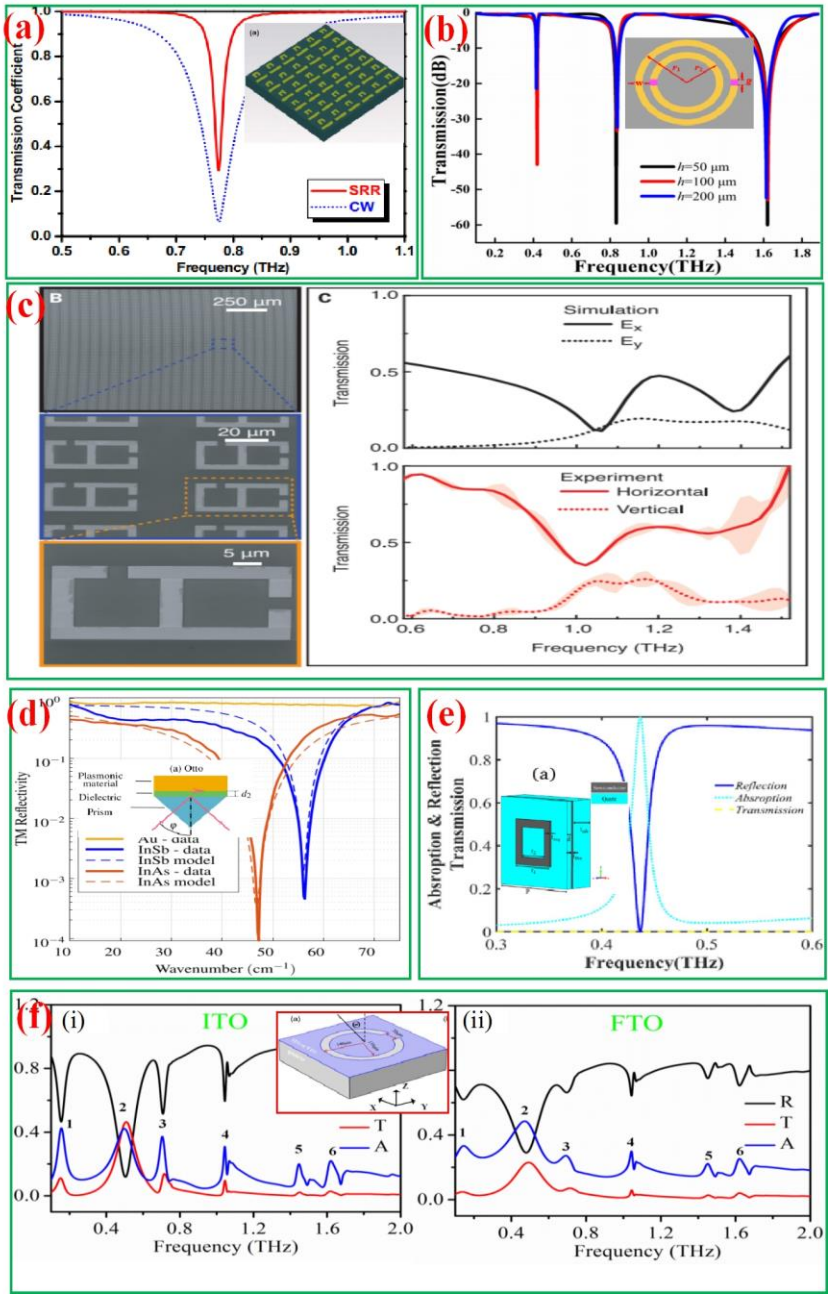

Figure 13: Terahertz metamaterials based on inorganic compound materials for sensing applications. (a) An InSb split-ring resonator with InSb wire and its performance characteristics [133]. (b) A schematic diagram of the metamaterial/perovskite hybrid structure and its terahertz transmission spectrum [139]. (c) Transmission spectra of the InP terahertz metamaterial [140]. (d) SPRs of the InSb and InAs compounds with transverse magnetic (TM) reflectivity measured in the terahertz frequency range [134]. (e) Three-dimensional structure of the metamaterial sensor and its transmission, reflectivity, and absorption spectra [56]. (f) The computed frequency-dependent reflection, transmission, and absorption of (i) ITO and (ii) FTO CSRRs metasurfaces [141].

Table 7: Recent applications of the TMS techniques based on inorganic compound materials

Inorganic Compound Materials (InAs, InSb, ITO, and Perovskites)				
Application	Target	Technique	Main results	Materials and reference
Terahertz sensing	N/A	Semiconductor split-ring resonator	Thermally tunable resonators	InSb [142a]
	N/A	Planar semiconductor metamaterial	Continuously tunable broad frequency	InSb [133a]
	N/A	Terahertz plasmonic response	46.7% transmittance modulation	InSb [135a]
	N/A	Terahertz plasmonic response	Strong field enhancement	InSb [136a,b]
	N/A	Fano resonance	Highly sensitive modulation	Perovskites [138a,b]
	N/A	Perovskite split-ring resonator	Modulation depth > 99%	Perovskites [139a]
	N/A	InP twisted split-ring resonator pair	Polarization sensitive	InP [140a,b]
Biomedical science	Thin films	SPR	Tunable sensitivity	InSb + InAs [134a,b]
	Biomolecules	Semiconductor metamaterial perfect absorber	S= 146600 nm/RIU	InSb [56a]
	Thin films	Broadband metasurface absorber	Absorbance of over 80%	ITO [137a]

[a] (simulation); [b] (experiment)

3.2.2 Organic Compound Materials

The fabrication of flexible electronic devices requires lightweight and highly processable metamaterials, which cannot be obtained from metallic, two-dimensional, or inorganic materials. In addition, various metamaterial patterns may be easily produced from organic materials using modern printing technologies. Based on the recent success of organic materials in fabricating large-area and flexible electronic devices, it is reasonable to consider them for producing organic compound metamaterials for terahertz sensing[143].

For example, Matsui et al. investigated the terahertz transmission modulation through a 200 nm copper phthalocyanine thin film by terahertz-TDS[144] (**Figure 14(a)).** Gu et al. designed an absorber containing a 4-N,N-dimethylamino-4′-N′-methyl-stilbazolium tosylate (DAST) crystalline film (**Figure 14(b)**)[145]. Nearly perfect terahertz absorption was observed for a 4 μm thin DAST film, which allowed tuning the terahertz signal response by adjusting its thickness. Zhang et al. reported a terahertz gas sensor based on the guided Bloch surface wave resonance in a one-dimensional photonic crystal, which consisted of the periodic polycarbonate (PC) and polyvinylidene fluoride (PVDF) layers (**Figure 14(c)**)[39]. The calculated angular sensitivity of HCN hazardous gas was 118.6°/RIU, and the obtained frequency sensitivity was 4.7 terahertz/RIU. Hence, the described designs may be used for detecting dangerous and hazardous gases. Table 8 summarizes the recent applications of the TMS techniques based on organic compound materials. For instance, the exploitation of organic compound materials for detection of THz waves is also at its early stage. However, for TMS made from PC and PVDF shows relatively high sensitivity. Considering the low cost、stable and reusable properties of this all-polymeric THz sensor, they are promising for the commercial applications of terahertz metamaterial sensors.

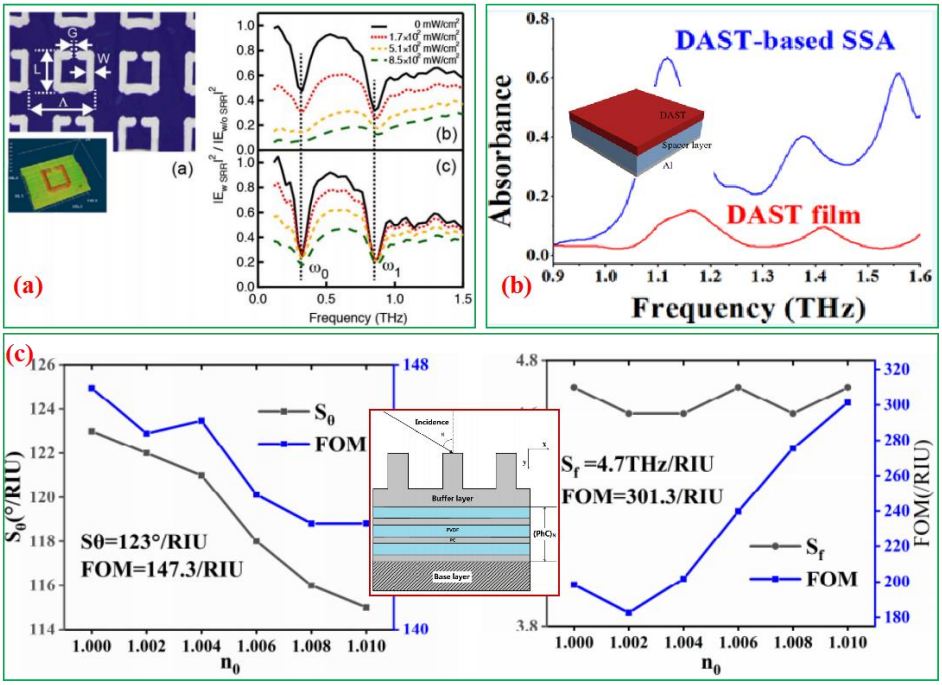

Figure 14: Terahertz metamaterials based on organic compound materials for sensing applications. (a) A split-ring resonator array on a 200-nm copper phthalocyanine film and its performance characteristics [144]. (b) A DAST-based Salisbury screen absorber and its Terahertz absorbance spectra [145]. (c) Schematic illustration of the dielectric multilayer consisting of nine alternating dielectric PC (7 μm) and PVDF (5 μm) layers [39]. Sensitivity and FOM values obtained from the transmission spectra of gases with different refractive indexes.

Table 8: Recent applications of the TMS techniques based on organic compound materials

Organic Compound Materials (Copper Phthalocyanine, PVDF, PC, and DAST)				
Application	Target	Technique	Main results	Materials and reference
Terahertz sensing	N/A	Organic materials split-ring resonator	Photo-induced efficient modulation	Copper phthalocyanine [144a]
	N/A	Salisbury screen absorber	Perfect Terahertz absorption	DAST [145a,b]
	N/A	Organic Terahertz modulator	High modulation factor	Phthalocyanine compound [146a]
Biomedical science	Hazardous HCN gas	Guided Bloch surface wave resonance	Frequency sensitivity of 4.7 Terahertz/RIU FOM of 301.3	PC + PVDF [147a]

[a] (simulation); [b] (experiment)

3.3 Hybrid Metamaterials

As of today, the sensitivity of label-free terahertz sensing for detecting trace amounts of target substances and molecular vibrations remains relatively low. The generation of resonantly enhanced electromagnetic fields in hybrid metamaterials represents a potential solution to this problem, albeit a highly complicated one[21-23]. Consequently, hybrid metamaterials are attracting increasing interest from researchers because they possess the advantages of several artificial magnetic materials, which can play a key role in the TMS process[24,25,148-159]. For example, the hybrid metamaterials containing Au and graphene components combine the high sensitivity of Au with the dynamic tunability of graphene[22,25,155]. The excellent performance characteristics of terahertz hybrid metamaterials make them applicable in biomedical science and environmental monitoring with a possibility of further structural optimization for property enhancement[157,158,160]. Note that the majority of tunable hybrid metamaterials are graphene-based materials.

For example, to increase the TMS sensitivity and meet the requirements of many biomedical research application areas (including early disease diagnostics and pharmacology), Zeng et al. developed a novel hybrid graphene/gold metasurface architecture (**Figure 15(a)**)[25]. This architecture exhibited enhanced sensitivity and enabled the detection of trace amounts of single-stranded DNA molecules with a concentration of 1×10^{-18} M. Moreover, some Au nanomaterials may potentially have high detection sensitivity; however, they do not exhibit any terahertz plasmonic activity and therefore, cannot be directly used in terahertz sensing. To address this issue, Xu et al. introduced Au nanoparticles into terahertz avidin metamaterial to increase its sensitivity

for protein detection (**Figure 15(b)**) [23]. The limit of detection of the conjugated avidin - Au nanoparticle structure was 7.8 fmol, which represented a 1000-fold improvement when compared with that of avidin alone. Furthermore, to increase the sensitivity of detecting molecular vibrations in the low-energy terahertz region, Bui et al. used a micrometer-scale, thin-slab metamaterial architecture of the Ag-Si-Ag tri-layered structure presented in **Figure 15(c)** [147], which enhanced the vibrational fingerprints of organic molecules at the resonance frequency. Finally, Xu et al. designed a simple biosensing platform by adding a graphene monolayer onto the surface of a terahertz metamaterial absorber cavity to make it more sensitive (**Figure 15(d)**) [22]. The resulting sensitivity of detecting trace amounts of chlorpyrifos methyl was as low as 0.2 ng. The recent applications of the TMS techniques based on hybrid metamaterials are summarized in Table 9. Hybrid metamaterials with resonantly enhanced electromagnetic fields offer a potentially viable, but complex solution. Consequently, hybrid metamaterials can combine the advantages of several artificial magnetic materials with good TMS characteristics. By optimizing the architecture of hybrid metamaterials, their TMS sensitivity and tunability in the terahertz range have been considerably increased.

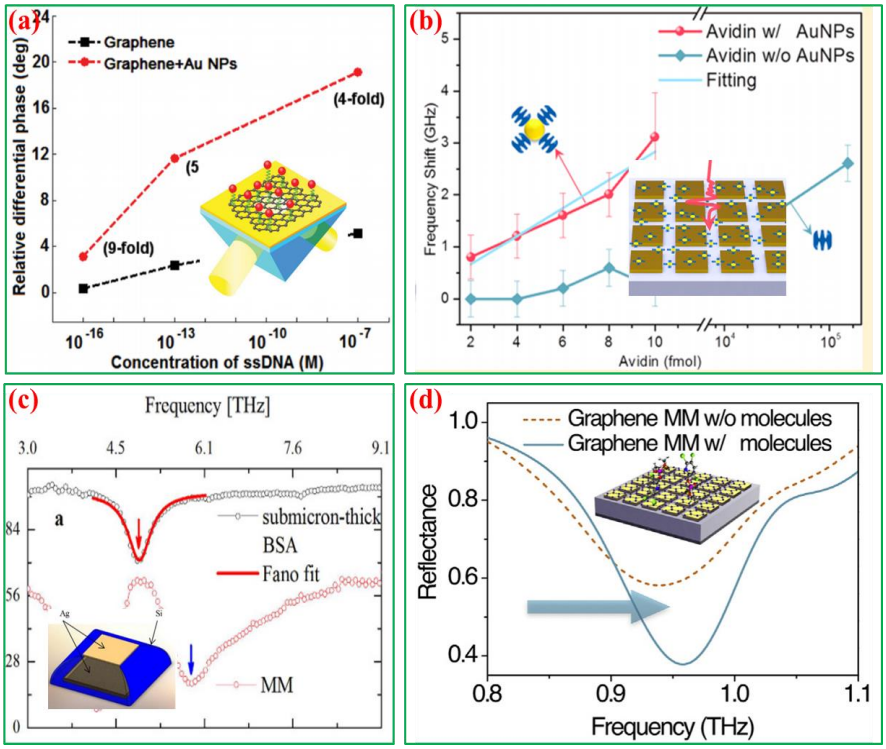

Figure 15: Terahertz sensing techniques based on the hybrid metamaterials for biomedical science and environmental monitoring applications. (a) Hybrid graphene/gold metasurface architectures [25]. (b) Gold nanoparticle detection by Terahertz metamaterials[23]. (c) Ag disk arrays used as the back and top resonators for sandwiching a Si insulator [147]. (d) Terahertz reflection spectra of the monolayer graphene-coated metamaterials with/without chlorpyrifos-methyl molecules [22].

Table 9: Recent applications of the TMS techniques based on hybrid metamaterials

	Target	Technique	Main results	Reference
Terahertz sensing	Thin films	Si nanodisk array + gold film	*S*= 350 nm/RIU	[21[a]]
	Thin films	Al_2O_3 ultra-thin layer+Au annular gap array	Detection of 1 nm dielectric layer	[148[a,b]]
	Thin films	Zeonex +graphene pattern	Absorption of 99.7%	[149[a]]
	N/A	Reduced graphene oxide ribbons + patterned graphene	Enhanced sensitivity	[150[a,b]]
	Thin films	Labyrinth metasurface absorber	Sensitivity of 800	[151[a,b]]
	N/A	Graphene structure + metal	High performance	[24[a,b]]
	N/A	Graphene disk + an annular gold ring	Sensitivity of 1.9082 Terahertz/RIU	[152[a]]
	N/A	Graphene-silicon metasurface	High modulation	[153[a,b]]
	Thin films	Graphene monolayer + Al asymmetric spit-ring resonators	Analyte detection is $\lambda/10^6$ thinner than Terahertz wavelengths	[154[a,b]]

	N/A	Graphene–gold Fano resonator	Ultra-sensitive bio-detector	[155[a]]
	N/A	CNTs + Au spit-ring resonators	Sensor for anisotropic materials	[156[a,b]]
Biomedical science	Lactose molecules	Monolayer graphene + Cu nanoslot	Detection of an ultra-small number of molecules	[157[b]]
	Thin lactose layers	Microrod array on lithium niobite surface	Highly sensitive on-chip Terahertz sensor for detecting trace amounts	[158[a,b]]
	Avidin detection	Gold nanoparticles + Terahertz metamaterial	Detection limit of 7.8 fmol	[23[a,b]]
	Biomolecules	Graphene + gold metasurface	S= 1 × 10^{-18} M for DNA	[25[a,b]]
	Protein molecules	Ag-Si-Ag +metamaterial	Terahertz vibrational sensing of large biomolecules	[147[a,b]]
	Water	Graphene/waveguide hybrid structure	Sensitivity of 3260 /RIU	[159[a,b]]
Environ	Acetone gas	Split-ring metasurface + cellulose foam	High Q-factor	[160[a,b]]
	Chlorpyrifos-methyl species	Monolayer graphene + Au patch resonator array	Sensitivity as low as 0.2 ng	[22[a,b]]

[a] (simulation); [b] (experiment)

4. TMS Substrate Materials

TMS devices are usually fabricated on semiconductor or dielectric substrates, which strongly interact with the metamaterial and thus contribute to the observed resonance shifts. The overall capacitance of such devices can be expressed as follows[161]:

$$c = c_1 + c_2 + c_3 + c_4 \quad (7)$$

where c_1 is the substrate capacitance, c_2 is the capacitance of the region between the substrate and the metamaterial, c_3 is the metamaterial capacitance, and c_4 is the capacitance of the region between the metamaterial and the sample. Hence, the substrate with high resistance, high dielectric constant, and large thickness exhibits a relatively large c_1 value and, therefore, relatively smaller changes in the capacitance of the metamaterial due to its low overall sensitivity. To increase the overall sensitivity of a

TMS device, we should minimize the substrate capacitance contribution by using substrates with low dielectric constants, absorption losses, and thicknesses.

4.1 Hard Substrates

The recent advances in the development of TMS devices with different substrate materials are summarized in Table 10. Some of these devices are fabricated on hard substrates, while the other devices are fabricated on flexible substrates. The hard substrate materials for TMS applications include silicon[1,2,5,54,68,81,84,100,119,149,150,153,154], gallium arsenide[60,135,136,162], glass[113,148], SiO_2[21,55,98–101,104,107,152], quartz[56,91,133,142], AlN[168], SiN_x[65], and sapphire[147]. They are usually characterized by the high permittivity and high resistance (such as those of silicon and gallium arsenide). Park et al. developed a highly sensitive detector of viruses consisting of a terahertz Au split-ring on a silicon substrate (**Figure 16(a)**)[68]. As shown in Table 10, the TMS devices based on common metals are usually fabricated on silicon substrates because of the high compatibility of silicon with such common metals. Moreover, silicon substrates are suitable for the processing of common and noble metal-based metamaterials conducted at high temperatures and pressures during preparation. **Figure 16(b)** displays the tunable terahertz sensor containing the graphene disk with an annular golden ring on a SiO_2 substrate fabricated by Zhang et al.[152]. Their work (also referenced in Table 10) indicates that graphene-based TMS devices are usually fabricated on SiO_2 substrates because the latter allows easy voltage application to the graphene layer to adjust its conductivity and thus, test the device performance characteristics. In addition to the silicon and silicon

dioxide substrates, GaAs, glass, and silicon nitride are often used as TMS substrate materials (**Figures 16(c, d)**) [65,158,162].

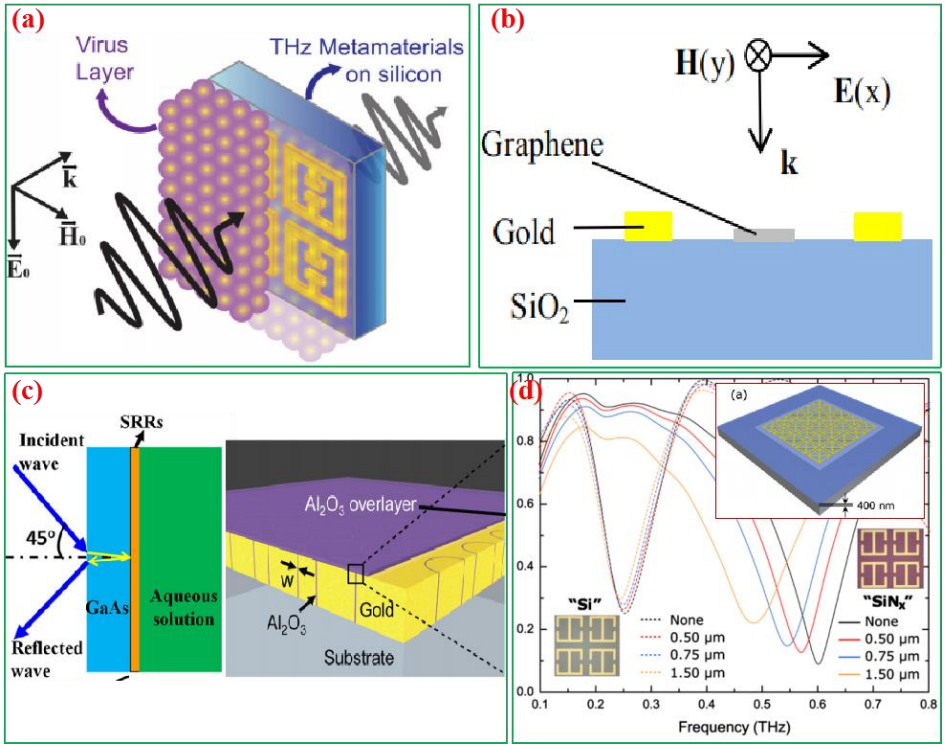

Figure 16: TMS devices containing hard substrates. (a) A Terahertz split-ring resonator on a silicon substrate [68]. (b) Graphene disk and annular gold ring within a unit cell on a SiO_2 substrate [152]. (c) Au split-ring resonators fabricated on a GaAs substrate and an Al_2O_3 ultra-thin layer on the annular Au gap array deposited on a glass substrate [162]. (d) A metal planar split-ring resonator fabricated on a thin silicon nitride substrate [65].

4.2 Flexible Substrates

The structures of the flexible substrates for TMS devices are agile and diverse; therefore, these substrates can be arranged according to the measurement conditions. In addition, the small size, integrated structure, and intelligence of flexible TMS devices facilitate the detection of particular signals in a specific environment. Thus, such devices play important roles in various areas, including biomedicine, wearable electronics, and aerospace[163,164,166,167]. The flexible substrate materials used for TMS devices generally

consist of polyimide[22-24,26,66], polyethylene terephthalate[67], polypropylene[169], paper [163], polydimethylsiloxane[166], silk[164], and $NiAl_2O_4$[167]. Zhang et al. proposed a terahertz metamaterial-based biosensor fabricated on a polyimide substrate (**Figure 17(a)**)[66]. Yang et al. developed a terahertz metamaterial biosensor on an ultra-thin polyethylene terephthalate substrate (**Figure 17(b)**)[68]. In addition to the commonly used polyimide and polyethylene terephthalate flexible substrates, many other flexible materials can be employed as the TMS substrates for planar metallic resonators with good performance characteristics, such as paper, silk, and benzocyclobutane (**Figures 17(c-e)**) [163-165].

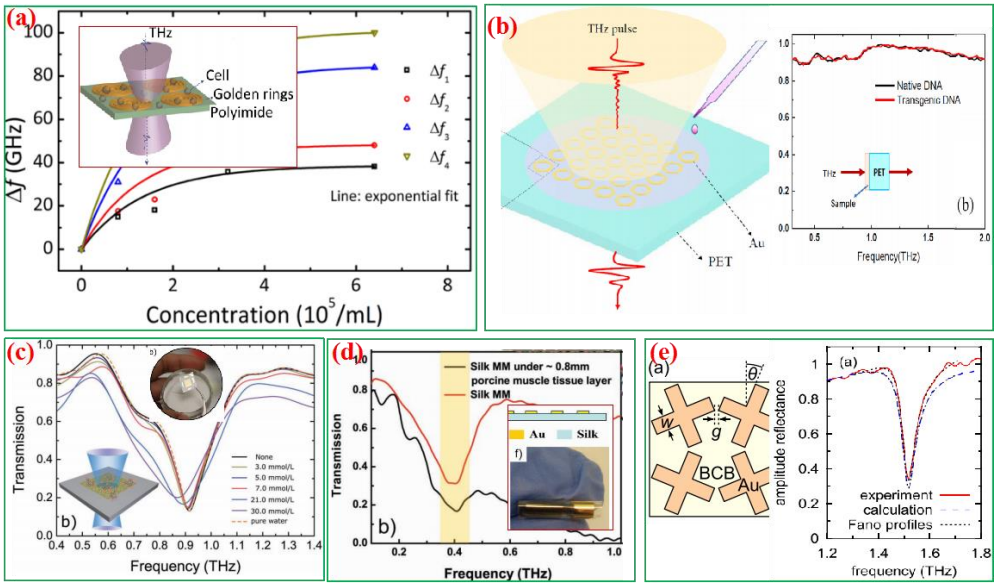

Figure 17: TMS devices fabricated on flexible substrates. (a) A planar array of the five concentric sub-wavelength golden ring resonators on a polyimide substrate [66]. (b) A planar array of the golden split-ring resonators on a polyethylene terephthalate substrate[67]. (c) Micrometer-sized metamaterial resonators sprayed on a paper substrate[163]. (d) Terahertz metamaterials on silk substrates [164]. (e) Four metallic crosses on a benzocyclobutane substrate [165].

Table 10: Recent applications of the TMS devices with various substrate materials

Substrate material	References

Hard substrates	Silicon	[1,2,5,54,68,81,83,100,119,149, 153,154]
	Glass	[113,146]
	SiN_x	[65]
	SiO_2	[21,54,98–101,104,107,152]
	Quartz	[56,91,133,142]
	AlN	[168]
	Sapphire	[148]
	Polytetrafluoroethylene	[60,135,136,162]
	Gallium arsenide	[22–24,26,66]
Flexible substrates	Polyimide	[67]
	Polyethylene terephthalate	[162]
	Benzocyclobutane	[166]
	Paper	[163]
	Polydimethylsiloxane	[167]
	Silk	[169]
	$NiAl_2O_4$	[1,2,5,54,68,81,84,100,119,149,150,153,154]
	Polypropylene	[113,148]

5. Conclusions and Perspectives

Over the past several decades, significant progress has been made in the development of various metamaterials and substrates for TMS applications. These materials suggest new approaches for studying the structural, functional, and sensing characteristics of TMS devices as well as their correlations with the sensor performance. In this paper, we reviewed the widely used TMS metamaterial components, including single-element materials (common and noble metals, graphene, CNTs, BP, and silicon), inorganic and organic compound materials, hybrid materials, and substrate materials (both hard and flexible ones). The applicability range and uniqueness of each material were identified, and the main parameters of the corresponding TMS techniques were described. Table 11 lists the characteristics of various TMS materials reviewed in this work. Unfortunately, most of the THz metamaterials based sensors as introduced in this review paper have not

been fully or partially commercialized, due to some potential reasons as detailed below: (1) For TMS made from noble and common metals, the cost of lithography process with high forming precision is very expensive; (2) For TMS made from two-dimensional single element materials, the cost of material itself is relatively high such as graphene (several hundred dollars per gram) and the non-reusability of materials also pushes up the cost of sensors; (3) For TMS made from silicon and organic materials, the sensitivity of these kinds of sensors are usually low. Therefore, for the commercial applications of terahertz metamaterial sensors, it is very promising to use all-polymeric THz sensing materials with low cost, stable and reusable properties [39].

Table 11: Characteristics of the TMS materials discussed in this paper

Materials		Dissipation	Stability	Cost	Sensitivity
Noble and Common Metals		High	High	High in Lithography process [170]	High
Two-dimensional Single Element Materials	Graphene	Middle	Low	High in Graphene [95-100]	Very High
	CNTs	Middle	High	High in CVD process[113-115]	Low
	BP	Middle	Low	High in BP [91-92, 121-122]	Median
Silicon		Low	High	Low	Low
Compound Materials	Inorganic Materials	Low	High	Low	Median
	Organic Materials	Middle	Low	Low	Low
Hybrid Materials		Depends	Depends	High	Very High
Substrates Materials	Hard Substrates	High	High	Depends	NA
	Flexible Substrates	Low	High	Depends	NA

5.1 Noble and common metals

Noble and common metals (such as Au, Al, Ag, and Cu) with SPR characteristics are the

most extensively studied materials in the terahertz regime for sensing applications. In addition, metal-containing TMS sensors can be easily combined with microfluidic channels and the ATR technique to increase their sensitivity and provide more accurate biomolecule information. However, in practical applications (especially those related to medical diagnostics), the relatively high absorption losses and dynamically non-tunable properties of these sensors remain a serious issue. Absorption losses can be mitigated by implementing some passive approaches. Such materials include metasurfaces consisting of organic dyes and semiconductors[171, 172]. Meanwhile, to realize dynamically tunable terahertz sensors, strong optical nonlinear materials can be integrated with metal metamaterials for permittivity tuning using the Kerr effect. In addition, phase-change materials, such as liquid crystals and transition-metal oxides, may be also utilized to tune metal metamaterial's permittivity by applying an external electric voltage [171].

5.2 Two-dimensional Single-element Materials

The two-dimensional single-element materials include graphene, CNTs, and BP. The terahertz responses of such materials can be dynamically tuned by applying an external electric voltage, and their intrinsic losses are relatively low as compared with those of common and noble metals. The TMS devices based on two-dimensional single-element materials are characterized by small volumes, high sensitivities, and fast responses. Additionally, the good compatibility of the described materials with silicon electronics and photonics may allow their integration with these technologies in the future. However, single sheets of two-dimensional single-element materials exhibit poor absorption

characteristics; therefore, their combinations with nanomaterials/nanostructures may help create TMS metamaterials with unique properties and ultrahigh sensitivity[173]. Moreover, the sensing mechanisms of the molecules adsorbed on the graphene, CNT, and BP surfaces and their interactions must be studied in more detail [174].

5.3 Silicon

Silicon has attracted much interest from researchers as a TMS material because silicon metastructures can overcome the poor applicability of graphene and BP and the intrinsic absorption losses observed for common and noble metals. Moreover, silicon can be easily integrated with silicon-based photonic platforms using the existing CMOS technology due to its tunable conductivity. However, the sensitivity and accuracy of silicon-based TMS requires further improvement for the development of low-cost fast sensors. Novel silicon metamaterial designs such as Fano-like structures and metamaterial absorbers may be potentially used in ultra-sensitive applications. After the development of fluidic manipulation technologies (especially microfluidic and nanofluidic ones), it may be possible to prepare silicon-based metafluidic metamaterials with high detection sensitivity and accuracy.

5.4 Multi-element Materials

The multi-element materials used in TMS applications include inorganic and organic materials. Their advantages include high reusability and the ability to actively tune plasma frequencies by varying the carrier concentrations. Meanwhile, organic metamaterials for terahertz sensing exhibit high scalability, low weights, and good

processability properties, which are critical for some practical applications. There are ongoing studies aimed at exploring various inorganic and organic compound materials for TMS. However, the foundational knowledge that can help to determine the prerequisites for obtaining inorganic and organic metamaterial films with negative permittivity and negative permeability must be expanded to enhance the performance of terahertz metamaterial sensors.

5.5 Hybrid Materials

Currently, the sensitivities of label-free terahertz sensing devices for detecting trace amounts of target substances and molecular vibrations are relatively low[175]. Hybrid metamaterials with resonantly enhanced electromagnetic fields offer a potentially viable, but complex solution. Consequently, hybrid metamaterials can combine the advantages of several artificial magnetic materials with good TMS characteristics. By optimizing the architecture of hybrid metamaterials, their TMS sensitivity and tunability in the terahertz range have been considerably increased. However, terahertz sensing based on hybrid metamaterials is a relatively new technology, and additional studies must be performed to elucidate the theoretical and experimental hybrid effects. A good starting point would include the identification of targets with multi-resonance peaks, which may help to improve the detection accuracy. Therefore, the hybrid metamaterials characterized by multi-resonance peaks are expected to attract more attention in the future.

5.6 Substrate Materials

TMS devices are usually manufactured on semiconductor or dielectric substrates, which

also cause resonance shifts due to their interactions with metamaterials. Some devices are fabricated on hard substrates, while other devices are made on flexible substrates. High TMS sensitivity can be achieved by designing ultra-thin substrates with low permittivity, such as those produced from silicon nitride and commercial paper. However, the sensitivity and accuracy of the resulting TMS devices must be further increased for their practical implementation. In addition, selection of the most suitable substrate material is based on its performance characteristics, manufacturing cost, and reusability.

Moreover, the metamaterials specifically designed to resonate with the terahertz wave can be used to enhance the sample-wave interactions by a surface plasmon polariton like effect. However, the enhanced sample-wave interactions by metamaterials should not only be applied to the sensing field as discussed above, but also to the following fields just like the main research directions of our group. 1. Dynamic monitoring at molecular levels: TMS technology just as the magnifier to help us in understanding and relating the measurements of the molecular dynamic information. 2. Terahertz imaging: terahertz imaging is still in the early stages of development with much lower resolution and specificity. Therefore, one of the biggest unsolved problems in terahertz medical imaging is how to enhance terahertz image contrast and suppress noise effects. TMS technology is able to enhance the sample-wave interactions by a surface plasmon polariton like effect.

A roadmap of some representative metamaterials in recent 10 years discussed in this paper is given in **Figure 18**. For the realization of practical application based on TMS, new mechanisms (such as topological effects) and novel metastructures should still be

exploited to achieve higher sensitivity. More importantly, the compatibility and integration of the TMS on chips are a challenge.

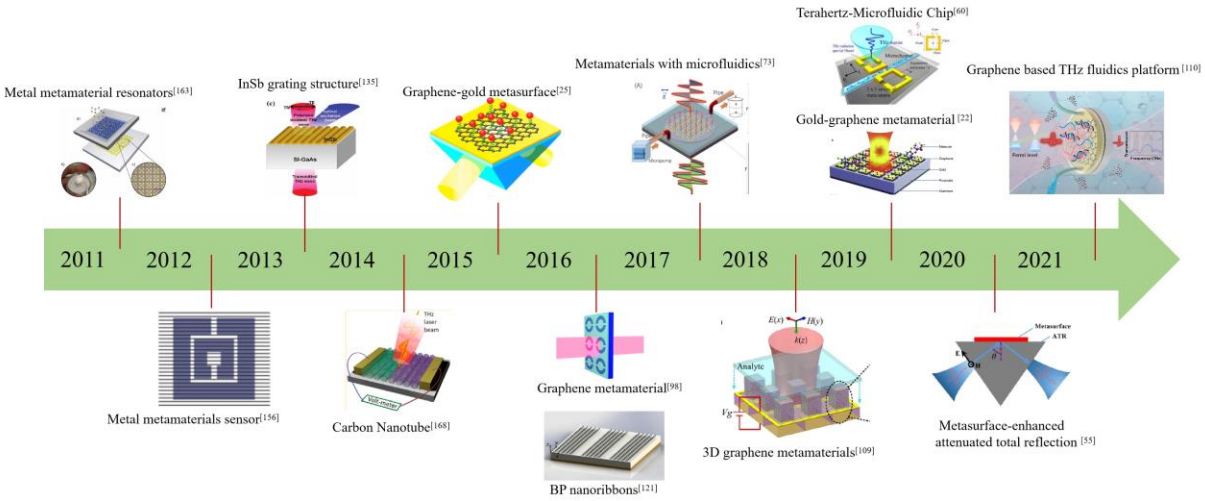

Figure 18: The roadmap of some representative metamaterials in recent 10 years.

Acknowledgements

The authors gratefully acknowledge the partial financial support for this work provided by the National Key Research and Development Program of China [grant number 2019YFC1604604], the National Natural Science Foundation of China [grant numbers 61805135, 61975148, 61275043, 61605128, 61425006], International Cooperation and Exchanges NSFC [grant number 61911530218], Natural Science Foundation of Guangdong Province [grant number 2019A1515010869], Shenzhen International Scientific and Technological Cooperation Project [grant number GJHZ20190822095407131], Basic and Applied Basic Research Foundation of Guangdong Province [grant number 2019A1515111007], SZU Start-up Fund [grant number 85304-00000334], Shenzhen High-end Talent Research Start-up Fund [grant

number 827-000366], SJTU Medicine Engineering Interdisciplinary Research Fund [grant number YG2017MS19], the Fundamental Research Funds for the Central Universities, the Royal Society Wolfson Merit Award (EPM), and the Engineering and Physical Sciences Research Council (EP/s021442/1).

Conflict of Interest

The authors declare no conflict of interest.

References

[1] P. Tassin, T. Koschny, C. M. Soukoulis, *Science* **2013**,341, 620.

[2] H. Zhou, C. Yang, D. Hu, D. Li, X. Hui, F. Zhang, M. Chen, X. Mu, *Appl. Phys. Lett.* **2019**, 115, 143507.

[3] W. Xu, L. Xie, J. Zhu, W. Wang, Z. Ye, Y. Ma, C.Y. Tsai, S. Chen, Y. Ying, *Food Chem.* **2017**,218 330.

[4] J. Qin, L. Xie, Y. Ying, *Food Chem.* **2016**, 211, 300.

[5] L. Cong, S. Tan, R. Yahiaoui, F. Yan, W. Zhang, R. Singh, *Appl. Phys. Lett.* **2015**, 106,031107.

[6] B. Ng, J. Wu, S. M. Hanham, A. I. Fernández-Domínguez, N. Klein, Y. F. Liew, M. B. H. Breese, M. Hong, S. A. Maier, *Adv. Optical Mater*. **2013**, 1, 543.

[7] Y. Sun, P. Du, X. Lu, P. Xie and R. Ullah*, *Spectrochimica Acta Part A-Molecular and Biomolecular Spectroscopy*, **2018**, 209, 70.

[8] Y. Wan，R. Zhang，H. Xiao, H. Wang，Y. Pan，Y. Zhou, *IEEE 2019 International Conference on Internet of Things.*

[9] T. J. Yen, W. J. Padilla, N. Fang, D. C. Vier, D. R. Smith, J. B. Pendry, D. N. Basov, X. Zhang, *Science* **2004**, 303, 1494.

[10] Y. Sun, J. Zhong, C. Zhang, J. Zuo, E. Pickwell-MacPherson, *J. Biomed. Opt*. **2015**, 20, 037006.

[11] M. Walther, B. M. Fischer, A. Ortner, A. Bitzer, A. Thoman, H. Helm, *Anal. Bioanal. Chem*. **2010**, 397, 1009.

[12] J. Qin, L. Xie, Y. Ying, *Anal. Chem*. **2014**, 86, 11750.

[13] F. M. Al-Douseri, Y. Chen, X. C. Zhang, *Int. J. Infrared. Milli*. **2006**, 27, 481.

[14] Y. Sun, Z. Zhu, S. Chen, J. Balakrishnan, D. Abbott, A. T. Ahuja, E. Pickwell-MacPherson, *PLoS ONE* **2011**, 7, 1.

[15] M. Janneh, A. D. Marcellis, E. Palange, A.T. Tenggara, D. Byun, *Opt. Commun*. **2018**, 416, 152.

[16] S. Banerjee, C.S. Amith, D. Kumar, G. Damarla, A. K. Chaudhary, S. Goel, B. P. Pal, D. R. Chowdhury, *Opt. Commun*. **2019**, 453, 124366.

[17] S. Banerjee, B. P. Pal, D. R. Chowdhury, *J. Electromagnet. Wave* **2020**, 1.

[18] Y. Wen, J. Zhou, *Mater. Today* **2019**, 37.

[19] M. Zhong, *Infrared Phys. Techn.* **2020**, 106,103264.

[20] Y. Zhang, Y. Feng, J. Zhao, *Carbon* **2020**,163, 244.
[21] H.T. Chen, *Opt. Express* **2012**, 20, 7165.
[22] W. Xu, L. Xie, J. Zhu, L. Tang, R. Singh, C. Wang, Y. Ma, H. Chen, Y. Ying, *Carbon* **2019**, 141, 247.
[23] W. Xu, L. Xie, J. Zhu, X. Xu, Z. Ye, C. Wang, Y. Ma, Y. Ying, *ACS Photonics* **2016**, 3, 2308.
[24] X. Yan, L. Liang, Z. Zhang, X. Ding, J. Q. Yao, *AOPC_2017: Optoelectronics and Micro/Nano-Optics.*
[25] S. Zeng, K. V. Sreekanth, J. Shang, T. Yu, C. Chen, F. Yin, D. Baillargeat, P. Coquet, H. Ho, A.V. Kabashin, K. Yong, *Adv. Mater*. **2015**, 27, 6163.
[26] X. Yan, M. Yang, Z. Zhang, L. Liang, D. Wei, M. Wang, M. Zhang, T. Wang, L. Liu, J. Xie, J. Yao, *Biosen. and Bioelectron.* **2019**, 126, 485.
[27] P. Tassin，T. Koschny，C. M. Soukoulis, *Science* **2013**, 314, 620.
[28] M. Zhong, X. Jiang, X. Zhu, J. Zhang, J. Zhong, *Opt. Laser Technol*. **2020**, 125, 106023.
[29] A. Houard，Y. Liu，B. Prade，V.T. Tikhonchuk，A. Mysyrowicz, *Phys. Rev. Lett*. **2008**, 100, 255006.
[30] H.T. Chen, W. J. Padilla, M. J. Cich, A. K. Azad, R. D. Averitt, A, J. Taylor, *Nature Photon*. **2009**, 3, 148.
[31] Y. Sun, P. Du, X. Lu, P. Xie, Z. Qian, S. Fan, Z. Zhu, Biomed. *Opt. Express* **2018**, 9, 2917.
[32] J. Qin, L. Xie, Y. Ying, *Food Chem*. **2015**, 170, 415.
[33] W. Pan, S. Huang, G. Li, T. Li, H. Tian, *Laser and Infrared* **2013**, 43, 438.
[34] H.T. Chen, R. Kerstin, G. C. Cho, *Appl. Phys. Lett.* **2003**, 83, 3009.
[35] V. G. Veselago, *Soviet Physics Uspekhi* **1968**, 10, 509.
[36] J. B. Pendry, A. J. Holden, W. J. Stewart, I. Youngs, *Phys. Rev. Lett.* **1996**, 76, 4773.
[37] J. B. Pendry, A. J. Holden, D. J. Robbins, *IEEE T. Microw. Theory* **1999**, 47, 2075.
[38] R. A. Shelby, D. R. Smith, S. C. Nemat-Nasser, S. Schultz, *Appl. Phys. Lett* **2002**, 78, 489.
[39] C. Zhang, S. Shen, M. Lin, Z. Ouyang, Q. Liu, *Materials* **2020**, 13, 1217.
[40] D. R. Smith, D. C. Vier, Th. Koschny, C. M. Soukoulis, *Phys. Rev*. **2005**, 71, 036617.
[41] R. Liu, C. Ji, J. J. Mock, J. Y. Chin, T. J. Cui, D. R. Smith, *Science* **2009**, 323, 366.
[42] T. J. Yen, W. J. Padilla, N. Fang, D. C. Vier, D. R. Smith, J. B. Pendry, D. N. Basov, X. Zhan, *Science* **2004**, 303, 1494.
[43] T. Driscoll, G. O. Andreev, D. N. Basov, *Appl. Phys. Lett*. **2007**, 91, 062511.
[44] W. J. Padilla, A. J. Taylor, *Phys. Rev. Lett*. **2006**, 96, 107401.
[45] R. Sun, W. Li , T. Meng, G. Zhao, *Optics Communications*, **2021**, 494, 127051.
[46] J. Li, J. Shao, Y. Wang, M. Zhu, J. Li, Z. Dong, *Opt. Express* **2015**, 23, 29138.
[47] T. Kaelberer, V. A. Fedotov, N. Papasimakis, D. P. Tsai, N. I. Zheludev, *Science* **2010**, 330, 1510.
[48] V. A. Fedotov, M. Rose, S. L. Prosvirnin, N. Papasimakis, N. I. Zheludev, *Phys. Rev. Lett.* **2007**, 99, 147401.
[49] R. Singh, I. A. I. Al-Naib, M. Koch, W. Zhang, *Opt. Express* **2011**, 19, 6312.
[50] Y. Qi, Y. Zhang, C. Liu, T. Zhang, B. Zhang, L. Wang, X. Deng, Y. Bai, X.Wang, *Results Phys.* **2020**, 16, 103012.
[51] S. Wang, X. Zhao, S. Wang, Q. Li, J. Zhu, L. Han, *J. Mater. Res*.**2020**, 9, 3935.

[52] P. Alitalo, S. Tretyakov, *Mater. Today* **2009**, 12, 22.
[53] L. Min, L. Huang, *Opt. Express* **2015**, 23, 19022.
[54] Y. Zhong , L. Du, Q. Liu, L. Zhu, B. Zhang, *Opt. Commun.* **2020**, 20, 30142.
[55] F. Yan , L. Li , R.Wang , H. Tian , J. Liu , J. Liu, F. Tian , J. Zhang, *J. Lightwave Technol*. **2019,** 37, 1103.
[56] M. Aslinezhad, *Opt. Commun*. **2020**, 463, 125411.
[57] A. Ren, A. Zahid, D. Fan, X.g Yang, M. A. Imrana, A. Alomainyc, Q. H. Abbasi, *Trends Food Sci. Technol*. 2019, 85, 241.
[58] L. Xie, W. Gao, J. Shu, Y. Ying, J. Kono, *Sci. Rep*. **2014**, 5, 8671.
[59] B. Hana, Z. Hanb, J. Qina, Y. Wang, Z. Zhao, *Talanta* **2019**, 192, 1.
[60] K. Serita, H. Murakami, I. Kawayama, M. Tonouchi, *Photonics* **2019**, 6, 12.
[61] R. Zhang, Q. Chen, K. Liu, Z. Chen, K. Li, X. Zhang, J. Xu , E. Pickwell-MacPherson, *IEEE T. Thz. sci. Techn.* **2019**, 9, 209.
[62] W. Xu, L. Xie, Y. Ying, *Nanoscale* **2017**, 9, 13864.
[63] J. A. Burrow, T. A. Searles, I. Agha1, *J. Mathews, Frontiers in Optics* **2017**.
[64] G. P. Papari, C. Koral, A. Andreone, *Sensors* **2019**, 19, 2544.
[65] H. Tao, A. C. Strikwerda, M. Liu, J. P. Mondia, E. Ekmekci, *Appl. Phys. Lett*. **2010**, 97, 261909.
[66] C. Zhang, L. Liang, L. Ding, B. Jin, Y. Hou, C. Li, L. Jiang, W. Liu, W. Hu, Y. Lu, L. Kang, W. Xu, J. Chen, P. Wu, *Appl. Phys. Lett*. **2016**, 108, 241105.
[67] Y. Yang, D. Xu, W. Zhang, *Opt. Express* **2018**, 26, 31589.
[68] S. J. Park, S. H. Cha, G. A. Shin, Y. H. AHN, *Biomed. Opt. Express* **2017**, 8, 3551.
[69] I. Jauregui I, P. Rodriguez-Ulibarri , S. A. Kuznetsov , M. Beruete, *10th International Congress on Advanced Electromagnetic Materials in Microwaves and Optics - Metamaterials* **2016**.
[70] L. L. Spada, *Sensors* **2019**, 19, 355.
[71] B. Wang, X. Zhai, G. Wang, W. Huang, L. Wang, *J. Appl. Phys*. **2015**, 117, 014504.
[72] M. Tonouchi, *Nature Photon*. **2007**, 1, 97.
[73] Z. Geng, X. Zhang, Z. Fan, X. Lv, H. Chen, *Sci. Rep*. **2017**, 7, 16378.
[74] S. Ramani, M. T. Reiten, P. L. Colestock, A. J. Taylor, Abul K. Azad, J. F. O'Hara, *IEEE Trans. Terahertz Sci. Technol*. **2013**, 3, 709.
[75] H. Hirori, K. Yamashita, M. Nagai and K. Tanaka, *JPN. J. Appl. Phys*. **2004**, 43, 1287.
[76] A. Ahmadivand, B. Gerislioglu, Z. Ramezani, A. Kaushik , P. Manickam, S.A. Ghoreishi, *Biosensors and Bioelectronics* **2021**, 177, 112971.
[77] T. L. Mako, J. M. Racicot, M. Levine, *Chem. Rev.* **2019**, 119, 322.
[78] J. Chen, F. Gan, Y. Wang, G. Li, *Adv. Optical Mater.* **2018**, 6, 1701152.
[79] M. F. Limonov, M. V. Rybin, A. N. Poddubny, Y. S. Kivshar, *Nature Photon.* **2017**, 11, 543.
[80] A.C. Das, *J. Inf. Sci. Eng*. **2018**, 7, 36.
[81] B. Orazbayev, N. M. Estakhri, A. Alù, M. Beruete, *Adv. Opt. Mater* **2017**, 5, 1600606.
[82] Y. He, Q. Wu, S. Yan, *Plasmonics* **2019**, 14, 1.
[83] C. Gao, L. Chen, J. Xu, Y. Zhu, *International Symposium on Photoelectronic Detection and Imaging: Terahertz Technologies and Applications 8909,* **2013**.
[84] R. Singh, W. Cao, I. Al-Naib, L. Cong, W. Withayachumnankul, W. Zhang, *Appl. Phys. Lett.*

2014, 105, 171101.
[85] I. Jáuregui-López, P. R. Ulibarri, S. A. Kuznetsov, N. A. Nikolaev, M. Beruete, *Sensors* **2018**, 18 3848.
[86] X. Hu, G. Xu, L. Wen, H. Wang, Y. Zhao, Y. Zhang, D. R. S. Cumming, Q. Chen, *Laser Photonics Rev*. **2017**, 10, 962.
[82] B. Ruan, J. Guo, L. Wu, J. Zhu, Q. You, X. Dai, Y. Xiang, *Sensors* **2017**, 17, 1924.
[88] Z. Sun, A. Martinez, F. Wang, *Nature Photon.* **2016**, 10, 227.
[89] S. Xu, L. L. Mou, F. Fan, S. Chen, Z. Zhao, D. Xiang, M. J. Andrade, Z. Liu, S. J. Chang, *Opt. Express* **2018**, 26, 28738.
[90] A.E. Nikolaenko, N. Papasimakis, A. Chipouline, F. De Angelis, E. Di Fabrizio, N.I. Zheludev, *Opt. Express* **2012**, 20, 6068.
[91] Q. Fo, L. Pan, X. Chen, Q. Xu, C. Ouyang, X. Zhang, Z. Tian, J. Gu, L. Liu, J. Han, W. Zhang, *IEEE Photon. J*. **2018**, 10, 4500709.
[92] Y. Qing, H. Ma, T. J. Cui, *Opt. Express* **2018**, 26, 32442.
[93] X. Liu, Z. Chen, E. P. J. Parrott, B. S.-Y. Ung, J. Xu, E. Pickwell-MacPherson, *Adv. Optical Mater.* **2017**, 5, 1600697
[94] X. Liu, Z. Chen, E. P. J. Parrott, B. Ung, J. Xu, E. Pickwell-MacPherson, *Adv. Optical Mater.* **2017**, 5, 1600697.
[95] A. Purkayastha, T. Srivastava, R. Jha, *Sens. Actuators B Chem.* **2016**, 227, 291.
[96] T. Srivastava, A. Purkayastha, R. Jha, *Opt. Quant. Electron* **2016**, 48, 334.
[97] Y. Xiang, J. Zhu, L. Wu, Q. You, B. Ruan, X. Dai, *IEEE Photon. J*. **2018**, 10, 6800507.
[98] W. Tang, L. Wang, X. Chen, C. Liu, A. Yu, W. Lu, *Nanoscale* **2016**, 8, 15196.
[99] Y. Xiang, X. Zhai, Q. Lin, S. Xia, M. Qin, L. Wang, *IEEE Photon. Technol. Lett.* **2018**, 30, 622.
[100] Q. Li, L. Cong, R. Singh, N. Xu, W. Cao, X. Zhang, Z. Tian, L. Du, J. Han, W. Zhang, *Nanoscale* **2016**, 8, 1.
[101] Z. Yia, J. Huanga, C. Cena, X. Chena, Z. Zhoua, Y. Tanga, B. Wangb, Y. Yic, J. Wangd, P. Wu, *Results Phys*. **2019**, 14, 102367.
[102] C. Fan, Y. Tian, P. Ren, W. Jia, *Chin. Phys. B*. **2019**, 28, 076105.
[103] M. Amin, M. Farhat, H. Bagci, *7th International Congress on Advanced Electromagnetic Materials in Microwaves and Optics- Metamaterials* **2013**.
[104] T. Yatooshi, A. Ishikawa, K. Tsuruta, *Appl. Phys. Lett.* **2015**, 107, 053105.
[105] R. Gao, Z. Xu, C. Ding, L.Wu, J. Yao, *Opt. Commun*. **2015**, 356, 400.
[106] H. Zhang, X. Huang, Q. Chen, C. Ding, T. Li, H. Lü, S. Xu, X. Zhang, Y. Zhang, J. Yao, *Acta Phys. Sin.* **2016**, 65, 018101.
[107] D. Rodrigo, O. Limaj, D. Janner, D. Etezadi, F. J. Abajo, V. Pruneri, H. Altug, *Science* **2015**, 349, 165.
[108] X. He, Q. Zhang, G. Lu, G. Ying, F. Wu, J. Jiang, *RSC Adv*. **2016**, 6, 52212.
[109] X. Chen, W. Fan, C. Song, *Carbon* **2018**, 133, 416.
[110] R. Zhou, C. Wang, Y. Huang, K. Huang, Y. Wang, W.Xu, L. Xie, Y. Ying, *Biosensors and Bioelectronics* **2021**, 188, 113336.
[111] R. Wang, L. Xie, S. Hameed, C. Wang, Y. Ying, *Carbon* **2018**, 132, 42.

[112] X. He, W. Gao, Q. Zhang, L. Ren, J. Kono, *Proc. of SPIE* **2015**, 9476, 947612.
[113] H. Park, S. Namgung, X. Chen, S. Oh, *Faraday Discuss*. **2015**, 178, 1951.
[114] R. Wang, W. Xu1, L. Xie, Y. Ying, *2019 44th International Conference on Infrared, Millimeter, and Terahertz Waves (IRMMW-THz)*.
[115] J. A. Russer, Y. Xiong, A. Abdellah, A. E. Culhaglu, W. Chet, P. Lugli, P. Russer, *2014 IEEE MTT-S International*, **2014**, 1.
[116] J. Wang, Y. Jiang, Z. Hu, *Opt. Express* **2017**, 25, 22149.
[117] J. Shi, Z. Li, D. K. Sang, Y. Xiang, J. Li, S. Zhang, H. Zhang, *J. Mater. Chem. C* **2018**, 6, 1291.
[118] Y. Lin, X. Liu, H. Chen, X. Guo, J. Pan, J. Yu, H. Zheng, H. Guan, H. Lu, Y. Zhong, Y. Chen, Y. Luo, W. Zhu, Z. Chen, *Opt. Express* **2019**, 27, 15868.
[119] L. Viti, J. Hu, D. Coquillat, W. Knap, A. Tredicucci, A. Politano, M. S. Vitiello, *Adv. Mater.* **2015**, 27, 5567.
[120] L.Viti, J.Hu, D. Coquillat, A. Politano, W. Knap, M. S.Vitiello, *Sci. Rep*. **2016**, 6, 20474.
[121] Z. Liu, K. Aydin, *Nano Lett*. **2016**, 16, 3457.
[122] T. Wang, L. Qu, L. Qu, Y. Zhang, H. Zhang, M. Cao, *J. Phys. D: Appl. Phys*. **2020**, 14, 1.
[123] I. Staude, J. Schilling, *Nature Photon*. **2017**, 11, 274.
[124] X. Zhao, Y. Wang, J. Schalch, G. Duan, K. Cremin, J. Zhang, C. Chen, R. D. Averitt, X. Zhang, *ACS Photon*.**2019**, 6, 830.
[125] H. Liu, K. Luo, S. Tang, D. Peng, F. Hu, L. Tu, *Materials* **2018**, 11, 2590.
[126] M. A. Hoeh, J. Neua, K. M. Schmitta, M. Rahm, *2014 39th International Conference on Infrared, Millimeter, and Terahertz waves (IRMMW-THz).*
[127] Y. Wang, D. Zhu, Z. Cui, L. Hou, L. Lin, F. Qu, X. Liu, P. Nie, *ACS Omega* **2019**, 4, 18645.
[128] J. Zhang, Y. Zhang, K. Gao, Y. Du, N. Zhang , Y. Lu, *Sci. China Tech. Sci*. **2013**, 56, 2238.
[129] K. Fan, J. Y. Suen, X. Liu, W. J. Padilla, *Optica* **2017**, 4, 601.
[130] A. Howes, W. Wang, I. Kravchenko, J. Valentine, *Optica* **2018**, 5, 787.
[131] Y. Deng, X.Wang, Z. Gong, K. Dong, S. Lou, N. Pégard, K. B. Tom, F. Yang, Z. You, L. Waller, J.Yao, *Adv. Mater.* **2018**, 30, 1802632.
[132] S. Yin, J. Zhu, W. Xu, W. Jiang, J. Yuan, G.Yin, L. Xie, Y.Ying, . Y. Ma, *Appl. Phys. Lett.* **2015**, 107, 073903.
[133] Q. Bai, C. Liu, J. Chen, C. Cheng, M. Kang, H. Wang, *J.Appl.Phys*. **2009**, 107, 093104.
[134] J. Chochol, K. Postava, M. Čada, J. Pištora, *Sci. Rep*. **2017**, 7, 13117.
[135] L. Deng, J. Teng, H. Liu, Q. Wu, J. Tang, X. Zhang, S. A. Maier, K. P. Lim, C. Ngo, S. Yoon, S. Chua, *Adv. Optical Mater.* **2013**, 1, 128.
[136] S. M. Hanham, A. I. Fernández-Domínguez, J. H. Teng, S. S. Ang, K. P. Lim, S. F. Yoon, C. Y. Ngo, N. Klein, J. B. Pendry, S. A. Maier, *Adv. Mater.* **2012**, 24, 226.
[137] S. Shrestha, Y. Wang, A. C. Overvig, M. Lu, A. Stein, L.Negro, N. Yu, *ACS Photon*. **2018**, 5, 3526.
[138] M. Manjappa, Y. K. Srivastava, A. Solanki, A. Kumar, T. C. Sum, R. Singh, *Adv. Mater*. **2017**, 29, 1605881.
[139] K. Wang, J. Li, *Opt. Commun*. **2019**, 447, 1.

[140] K. Peng, D. Jevtics, F. Zhang, S. Sterzl, D. A. Damry, M. U. Rothmann, B. Guilhabert, M. J. Strain, H. H. Tan, L. M. Herz, L. Fu, M. D. Dawson, A. Hurtado, C. Jagadish, M. B. Johnston, *Science* **2020**, 368, 510.

[141] S. Shen, Q. Liu, X.Liu, J. Huang, M. Jia, J. Qu, Y. Shen, Y. Sun, *Appl. Phys. Express* **2020**, 13, 102002.

[142] J. Han, A. Lakhtakia, *J. Mod. Opt*. **2009**, 56, 554.

[143] B. Li, G. Sui, W.H. Zhong, *Adv. Mater.* **2009**, 21, 4176.

[144] T. Matsui, R. Takagi, K. Takano, M. Hangyo, *Opt. Lett*. **2013**, 38, 4632.

[145] Y. Gu, X. Xu, F. Wang, M. Zhang, X. Cheng, Y. Jiang, T. Fan, J. Xu, *ACS Omega* **2019**, 4, 9204.

[146] T. He, B. Zhang, J. Shen, M. Zang, T. Chen, Y. Hu, Y. Hou, *Appl. Phys. Lett*. **2015**, 106, 053303.

[147] T. S. Bui, T. D. Dao, L. H. Dang, L. D.Vu, A. Ohi, T. Nabatame, Y. Lee, T. Nagao, C.V. Hoang, *Sci. Rep*. **2016**, 6, 32123.

[148] H. Park, X. Chen, N. Nguyen, J. Peraire, S. Oh, *ACS Photon*. **2015**, 2, 417.

[149] M.S. Islam, J. Sultana, M. Biabanifard, Z. Vafapour, M.J. Nine, A. Dinovitser, C.M.B. Cordeiro, B.W.-H. Ng, D. Abbott, *Carbon* **2020**, 158, 559.

[150] D. Mencarelli, Y. Nishina, A. Ishikawa, L. Pierantoni, S. Bellucci, *Opt. Data Process. Storage* **2017**, 3, 89.

[151] I. Jáuregui-López, P. Rodríguez-Ulibarri, A. Urrutia, S. A. Kuznetsov, M. Beruete, *Phys. Status Solidi-R* **2018**, 10, 1800375.

[152] Y. Zhang, T. Li, B. Zeng, H. Zhang, H. Lv, X. Huang, W. Zhang, A. K. Azad, *Nanoscale* **2013**, 00, 1.

[153] Q. Li, Z. Tian, X. Zhang, N. Xu, R. Singh, J. Gu, P. Lv, L. Luo, S. Zhang, J. Han, W. Zhang, *Carbon* **2015**, 90, 146.

[154] Q. Li, L. Cong, R. Singh, N. Xu, W. Cao, X. Zhang, Z. Tian, L. Du, J. Han, W. Zhang, *Nanoscale* **2016**, 8, 1.

[155] M. Amin, M. Farhat, H. Bagcı, *Sci. Rep.* **2013**, 3, 2105.

[156] J. H. Woo, E. Choi, B. Kang, E. S. Kim, J. Kim, Y. U. Lee, T. Y. Hong, J. H. Kim, I. Lee, Y. H. Lee, J. W. Wu, *Opt. Express* **2012**, 20, 15440.

[157] G. Choi, S. J. Hong, Y. Bahk, *Sci. Rep*. **2019**, 9, 9749.

[158] R. Wang, Q. Wu, Y. Zhang, X. Xu, Q. Zhang, W. Zhao, B. Zhang, W. Cai, J. Yao, J. Xu, *Appl. Phys. Lett*. **2019**, 114, 121102.

[159] B. Ruan, J. Guo, L. Wu, J. Zhu, Q. You, X. Dai, Y. Xiang, *Sensors* **2017**, 17, 1924.

[160] H. Chen, Y. Cheng, C. Tsui, Y. Chiang, C. Kao, W. Wang, *Proc. of SPIE* **2020**, 10969, 109690S.

[161] J. F. O'Hara, R. Singh, I. Brener, E. Smirnova, J. Han, A. J. Taylor, W. Zhang, *Opt. Express* **2008**, 16, 1786.

[162] X. Wu, X. Pan, B. Quan, X. Xu, C. Gu, *Appl. Phys. Lett*. **2013**, 102, 151109.

[163] H. Tao, L. R. Chieffo, M. A. Brenckle, S. M. Siebert, M. Liu, A. C. Strikwerda, K. Fan, D. L. Kaplan, X. Zhang, R. D. Averitt, F. G. Omenetto, *Adv. Mater.* **2011**, 23, 3197.

[164] H. Tao, J. J. Amsden, A. C. Strikwerda, K. Fan, D. L. Kaplan, X. Zhang, R. D. Averitt, F. G. Omenetto, *Adv. Mater.* **2010**, 22, 3527.

[165] B. Reinhard, K. M. Schmitt, V. Wollrab, J. Neu, R. Beigang, M. Rahm, *Appl. Phys. Lett.* **2012**, 100, 221101.
[166] I. E. Khodasevych, C.M. Shah, W.S.T. Rowe, A. Mitchell, *Conference on Optoelectronic and Microelectronic Materials and Devices. IEEE*, **2010**.
[167] M. Rahman, E. Ahamed, M. R. Faruque, M. Islam, *Sci. Rep*. **2018**, 8, 14948.
[168] X. He, N. Fujimura, J. M. Lloyd, K.J. Erickson, A. A. Talin, Q. Zhang, W. Gao, Q. Jiang, Y.Kawano, R.H. Hauge, F. Leonard, J. Kono, *Nano Lett*. **2014**, 14, 3953.
[169] P. Rodrıguez-Ulibarri, S. A. Kuznetsov, M. Beruete, *Appl. Phys. Lett*. **2016**, 108, 111104.
[170] Z. Ren, Y. Chang, Y. Ma, K. Shih, B. Dong, C. Lee, *Adv. Optical Mater.* **2020**, 8, 1900653.
[171] P. Huo, S. Zhang, Y. Liang, Y. Lu, Ting Xu, *Adv. Optical Mater.* **2019**, 7, 1801616.
[172] Y. Lin, Z. Xu, *Int. J. Optomechatroni*. **2020**, 14,78.
[173] A. E. Minovich, A. E. Miroshnichenko, A. Y. Bykov, T. V. Murzina, D. N. Neshev, Y. S. Kivshar, *Laser Photonics Rev*. **2015**, 9, 195.
[174] R. Zhou, C. Wang, W. Xu, L. Xie, *Nanoscale* **2019**, 11, 3445.
[175] A. Ahmadivand, B. Gerislioglu, R. Ahuja, Y. K. Mishra, *Mater. Today* **2020**, 32, 108.

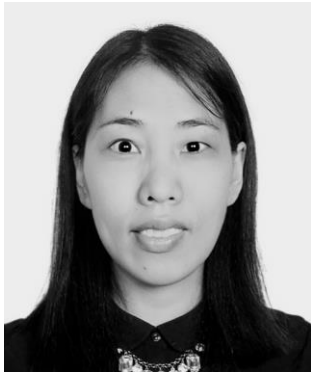

Suling Shen is currently working as postdoctoral researcher in the School of Medicine, Shenzhen University. She received the M.S. degree from the University of Chinese Academy of Sciences in 2010 and the Ph.D. degree in electronic engineering from the Chinese University of Hong Kong in 2017. Her current research interests include THz metamaterials, and their applications in bio-sensing, Terahertz characterizations.

Yiwen Sun received her Ph.D. degree in electronic engineering from the Chinese University of Hong Kong in 2010. Since then, she has been a full professor in the School of Medicine, Shenzhen University. Her research interests are focused on Terahertz metamaterial sensing, Terahertz biomedical sensing, Terahertz metrology and molecular dynamics analysis. Currently, she is the Deputy Secretary General of Biomedical Photonics Professional Committee of Chinese Optical Society.